

MICROCOPY RESOLUTION TEST CHART
NATIONAL BUREAU OF STANDARDS 1963-A

LEVEL

54

12

OCEAN-ATMOSPHERE INTERFACE: ITS INFLUENCE ON RADIATION

by

Gilbert N. Plass, Terry J. Humphreys and George W. Kattawar

Report No. 14

The research described in this report was

funded by

The Ocean Science and Technology Division

of the

Office of Naval Research

Contract N00014-80-C-0113

Department of Physics
Texas A&M University
College Station, Texas 77843

May 22, 1980

This report has been submitted to Applied Optics for publication.

This document has been approved
for public release and sale; its
distribution is unlimited.

DTIC
JUL 23 1980
C

ADA 087046

JDC FILE COPY

80 7 22 050

REPORT DOCUMENTATION PAGE		READ INSTRUCTIONS BEFORE COMPLETING FORM
1. REPORT NUMBER Report No. 14	2. GOVT ACCESSION NO. DD A087 046	3. RECIPIENT'S CATALOG NUMBER
4. TITLE (and Subtitle) OCEAN-ATMOSPHERE INTERFACE: ITS INFLUENCE ON RADIATION		5. TYPE OF REPORT & PERIOD COVERED Reprint of publication
7. AUTHOR(s) 1 Gilbert N. Plass, Terry J. Humphreys George W. Kattawar		6. PERFORMING ORG. REPORT NUMBER 14TR-141
9. PERFORMING ORGANIZATION NAME AND ADDRESS Department of Physics Texas A&M University College Station, Texas 77843		8. CONTRACT OR GRANT NUMBER(s) ONR Contract 15 N00014-80-C-0113 new
11. CONTROLLING OFFICE NAME AND ADDRESS Office of Naval Research Navy Department, Code 480 Arlington, VA 22217		10. PROGRAM ELEMENT, PROJECT, TASK AREA & WORK UNIT NUMBERS
14. MONITORING AGENCY NAME & ADDRESS (if different from Controlling Office)		12. REPORT DATE May 22 1980
		13. NUMBER OF PAGES 58
		15. SECURITY CLASS. (of this report) unclassified
		15a. DECLASSIFICATION/DOWNGRADING SCHEDULE
16. DISTRIBUTION STATEMENT (of this Report) The distribution of this report is unlimited.		
17. DISTRIBUTION STATEMENT (of the abstract entered in Block 20, if different from Report)		
18. SUPPLEMENTARY NOTES		
19. KEY WORDS (Continue on reverse side if necessary and identify by block number) Radiance, ocean, Rayleigh scattering, Mie scattering, absorption		
20. ABSTRACT (Continue on reverse side if necessary and identify by block number) The influence of the ocean-atmosphere interface on the radiance distribution in both the ocean and atmosphere is investigated. At visible wavelengths in the real ocean just below the surface, the downwelling radiance is a maximum within the critical angle and drops off by one or two orders of magnitude toward the horizon. The usual explanation that this is due to the sky radiation concentrated within the critical angle and the total internal reflection of the weak upward radiance at the ocean surface at angles outside the critical angle is too simplistic. There are two other important factors: (1) the atmosphere		

20. Abstract

must have sufficient optical thickness so that appreciable sky (multiple scattered) radiation develops at all angles in the downward direction; ^{AND} (2) the water must have appreciable absorption so that the upwelling radiance just below the ocean surface is only a small fraction of the downwelling radiance entering the ocean. Examples show that, if either one of these conditions is not satisfied, an entirely different radiance distribution develops. The variation of the following quantities with depth is studied: radiance, vector and scalar irradiance, distribution function, reflectance, and heating rate. The radiance distribution in a homogeneous medium is compared with that in the same medium with an atmosphere-ocean interface at various depths within the medium. Most of the calculations are done for Rayleigh scattering centers, but some results are given for Mie type scattering.

Accession	
NTIS	<input checked="" type="checkbox"/>
DDC TAB	<input type="checkbox"/>
Unannounced	<input type="checkbox"/>
Justification	
By	
Distribution	
Availability	
Dist	
A	

OCEAN-ATMOSPHERE INTERFACE: ITS INFLUENCE ON RADIATION

by

Gilbert N. Plass, Terry J. Humphreys and George W. Kattawar

ABSTRACT

The influence of the ocean-atmosphere interface on the radiance distribution in both the ocean and atmosphere is investigated. At visible wavelengths in the real ocean just below the surface, the downwelling radiance is a maximum within the critical angle and drops off by one or two orders of magnitude toward the horizon. The usual explanation that this is due to the sky radiation concentrated within the critical angle and the total internal reflection of the weak upward radiance at the ocean surface at angles outside the critical angle is too simplistic. There are two other important factors: 1. the atmosphere must have sufficient optical thickness so that appreciable sky (multiple scattered) radiation develops at all angles in the downward direction; 2. the water must have appreciable absorption so that the upwelling radiance just below the ocean surface is only a small fraction of the downwelling radiance entering the ocean. Examples show that, if either one of these conditions is not satisfied, an entirely different radiance distribution develops. The variation of the following quantities with depth is studied: radiance, vector and scalar irradiance, distribution function, reflectance, and heating rate. The radiance distribution in a homogeneous medium is compared with that in the same medium with an atmosphere-ocean interface at various depths within the medium. Most of the calculations are done for Rayleigh scattering centers, but some results are given for Mie type scattering.

The authors are with Texas A&M University, Physics Department,
College Station, Texas 77843.

I. Introduction

Divers marvel at the beautiful patterns of light visible within the ocean. When the surface is rough, it is difficult for the eye to provide information for a time-averaged radiance from the dancing points of light. On the other hand when the surface is calm, the entire world above the ocean is condensed by refraction of the rays at the surface into a cone extending from the zenith to the critical angle. If the surface is perfectly smooth, the radiance drops abruptly by one or two orders of magnitude as the viewing angle moves outside the critical angle. The usual explanation is that the sky radiation is concentrated within the critical angle in the ocean, while the downwelling radiation outside the critical angle is derived from the total internal reflection of the much weaker upwelling radiation just beneath the ocean surface.

Although this explanation is correct as far as it goes, it does not point out the dependence on several other properties of the medium. The influence of the absorption of the water in reducing the upwelling radiance within the ocean is crucial, as is the existence of a sufficiently deep atmosphere so that appreciable downwelling sky radiance develops. The dependence of the radiance distribution on these and the other optical properties of the medium is thoroughly explored in the following sections. For ease of calculation all results given in Sect. II - VII are for Rayleigh scattering. The effect of Mie-type scattering is illustrated in Sect. VIII. A smooth ocean surface is assumed for all these calculations.

II. Method of Calculation

The Matrix Operator Method was used for all calculations reported here. Theoretical expositions and applications of the theory to an inhomogenous medium have been previously presented by us.¹⁻³ The study of radiative transfer problems pertaining to the atmosphere-ocean system requires that the theory be modified to include reflection and refraction at the ocean's surface.

A new fundamental problem was encountered as a result of the attempt to implement these modifications. The problem encountered is a direct result of the law of refraction. In the standard matrix operator formalism, the set of zenith angles used for the purpose of calculation is derived from a quadrature; usually a set of abscissas equal to the positive points of either a Gauss or Lobatto quadrature. Within the modified theory, once a set of zenith angles is selected to represent either the atmosphere or the ocean, zenith angles (quadrature points) for the other region are specified by Snell's Law. No proven way of assigning weights to the non-linearly mapped points was available to us. For this reason, selection of the atmospheric quadrature, selection of the ocean quadrature and formulation of the mapping relating the weights of these quadratures was crucial to the implementation of the modified theory. All other problems related to inclusion of the dielectric interface, i.e. construction of reflection and transmission operators for the interface and phase function normalization criteria were attendant to or subordinant to this problem.

Four constraints arose naturally in the process of selecting the quadratures to represent the atmosphere-ocean system. First the quadrature for the atmosphere had to normalize a phase function adequate to represent scattering by atmospheric aerosols. Second, the ocean quadrature had to normalize the highly assymmetric phase functions used to represent hydrosol scattering. Third, the related quadratures had to guarantee conservation of energy transmitted and reflected by the dielectric interface. Finally, both the selected quadratures had to retain sufficient strength to integrate properly the intensity distributions arising in their respective regions.

Our solution to this problem was to use a set of M mapped Gauss points μ_j as our atmospheric quadrature. The quadrature points ξ_j within the ocean were then found by a simple application of Snell's Law, namely

$$\mu_j = [1 - (1 - \xi_j^2)n^2]^{1/2} \quad (1)$$

or

$$\xi_j = [1 - (1 - \mu_j^2)n^{-2}]^{1/2} \quad (2)$$

where μ_j are the cosines of the angles of incidence from above the interface, ξ_j are the cosines of the refracted angles within the ocean, and n is the index of refraction of water relative to air. The weights for these ocean quadrature points within the acceptance cone are found by

$$C_j^o = (\mu_j / \epsilon_j n^2) C_j^a, \quad (3)$$

where C_j^o is the calculated ocean quadrature weight corresponding to ϵ_j and C_j^a is the mapped Gauss weight of the corresponding atmospheric quadrature point μ_j . An additional set of K Gauss points was mapped into the regime from the critical angle to the horizon. A complete explanation of the reasoning behind these selections was presented by Kattawar, et al.⁴

With the quadrature types selected, solutions to all other problems were then simple to formulate. The minimum order of the atmospheric quadrature was determined by requiring it to allow the normalization of a chosen aerosol phase function to be within 0.05%. At the same time, the related ocean quadrature was required to normalize the necessary hydrosol phase function to similar accuracy. To minimize the size of the ocean quadrature necessary to normalize the hydrosol phase function, the delta function approximation used by Potter was employed.⁵

With suitable quadratures selected, the problem of constructing reflection and transmission operators to represent the interface properties became straightforward. For a scalar calculation they are merely diagonal matrices formed from the fresnel reflection and transmission coefficients, $r(\mu_j)$ and $t(\mu_j)$, for unpolarized radiation⁴ and a geometric factor derived from the change in solid angle on entry to or exit from the ocean.⁶ The reflection and transmission operators applicable to light traversing the interface from the atmosphere into the ocean may be written:

$$[R(A,W)]_{jk} = R(A,W)_j \delta_{jk} \quad , \quad (4)$$

$$[T(A,W)]_{jk} = n^2 T(A,W)_j \delta_{jk} \quad (5)$$

for $j = 1$ to M .

For light traversing the interface from the ocean into the atmosphere the reflection and transmission operators can be written:

$$[R(W,A)]_{jk} = R(W,A) \delta_{jk} \quad , \quad (6)$$

$$[T(W,A)]_{jk} = n^{-2} T(W,A)_j \delta_{jk} \quad , \quad (7)$$

for $j = 1$ to M ,

$$[R(W,A)]_{j-k'} = \delta_{j-k'} \quad , \quad (8)$$

$$[T(W,A)]_{j-k'} = 0 \quad , \quad (9)$$

for $j' = M + 1$ to $M + k$.

Completely new computer algorithms were implemented to accommodate the modifications to the method. The new algorithms perform both the co-decomposition of aerosol and hydrosol phase functions, and the radiation field calculations for a combined inhomogeneous atmosphere-ocean system. In addition facilities to allow calculation for any ocean bottom with a known reflectance have been built into the program. Two special features of particular value when studying radiative transfer

problems associated with the atmosphere-ocean system were also built into the program. The first allows the spectra from a complete wavelength scan to be calculated in a single run. The second allows calculations for multiple geometries to be made within a single run. The geometries of the second feature are limited to those which can be constructed by re-positioning the ground at the levels of any detectors imbedded in the ocean. Each aspect of the new code was tested by comparison to previous calculations^{1-3,7-9}.

III. Effect of Water Boundary

The radiance underwater has a distinct pattern well known to underwater swimmers and divers. When looking upward at the water surface, there is a bright pattern of light visible at zenith angles up to the critical angle, approximately 48° . By comparison the ocean appears very dark when viewed at zenith angles greater than the critical angle. This distribution is observed when the water surface is calm (waves smooth out the sharp drop in the radiance at the critical angle¹⁰), the bottom is not too near the surface, and the water is reasonably clear.

This usual underwater radiance distribution has been explained many times in the literature^{11,12}. All of the light from the sun and sky that enters the ocean is refracted into zenith angles less than the critical angle, while no light from the atmosphere can enter a calm ocean at greater angles. The upwelling light in the ocean just below the surface is always small in comparison to the downwelling. If this weak upwelling light encounters the ocean surface at angles greater than

the critical angle it is totally internally reflected and thus becomes downwelling light. This is the only source of downwelling light at angles greater than the critical angle and thus the downwelling light is weak outside the cone defined by the critical angle.

Although this explanation is correct as far as it goes, some details concerned us. A fundamental investigation of the manner in which the light field develops underwater seemed of interest. It soon became obvious that the situation is indeed more complicated in that other factors also control the light distribution. This is illustrated in Fig. 1, which shows the downward diffuse radiance just below the ocean surface as a function of the zenith angle of observation for a solar zenith angle, $\theta_0 = 11.44^\circ$. All radiance curves given in this article have been averaged over all azimuthal angles. There is no absorption in the atmosphere unless otherwise stated. Only Rayleigh scattering is assumed in both the atmosphere and ocean unless mentioned otherwise. This assumption greatly simplified the calculations and makes it easier to study the other factors that determine the underwater radiance distribution. The incoming solar radiation is normalized to unit flux through a surface perpendicular to the beam.

The top curve in Fig. 1 is for a set of parameters that corresponds to the actual ocean-atmosphere system at most visual wavelengths: the single scattering albedo (fraction of radiation actually scattered for each photon collision) of the ocean, $\omega_0 = 0.5$ and the optical depth of the atmosphere is taken as $\tau_{atm} = 0.5$. The ocean is assumed to be effectively of infinite depth. This radiance curve has the typical variation observed in the visible in the real ocean: the radiance is

relatively large for zenith angles of observation less than the critical angle and small at larger angles. There is a rapid change in the radiance near the critical angle.

If we merely change the single scattering albedo of the ocean from $\omega_0 = 0.5$ to $\omega_0 = 1$ and leave all the other parameters the same, an entirely different radiance curve is obtained, the bottom curve of this figure. With this change in the ocean albedo, the upwelling radiation is so much larger that, after total internal reflection at the water surface, the downwelling radiation observed beyond the critical angle is now much larger than the downwelling radiation from the sun and sky observed within the critical angle. Thus, the observed radiance curve in the ocean depends on the fact that the ocean water is a fairly good absorber of radiation at all visible wavelengths. If it were not, the radiance would have a maximum at angles greater than the critical angle.

Let us change just one other parameter in our original calculation. Instead of having a fairly substantial atmosphere above the ocean surface, let us have only a very thin atmosphere, $\tau_{\text{atm}} = 0.0001$. The radiance curve in the middle of the figure is obtained for this situation. Again the largest radiance values occur at angles of observation beyond the critical angle. These curves show only the diffuse radiance, i.e. photons which have been scattered one or more times from the direct solar beam. In this case, there are only a few photon collisions in the very thin atmospheric layer and there is virtually no sky radiation entering the ocean. Thus, the downwelling light observed just below the ocean surface is largely light from the upwelling radiation that has been internally reflected at the water surface and thus changed into downwelling radiation. At angles greater than the critical angle, all

of this radiation is reflected by total internal reflection. At angles less than the critical angle, the fraction reflected can be easily determined from the usual laws for reflection and is found to decrease rapidly as the angle of observation decreases from the critical angle. In this case, even though the ocean still has $\omega_0 = 0.5$, the radiance distribution is completely opposite from the observed one.

The conclusion from this brief example is that the observed radiance distribution in the ocean requires both (1) an atmosphere of reasonable optical thickness in order to develop appreciable sky radiation as well as (2) an ocean that absorbs an appreciable fraction of the photons. If either one of these requirements is not satisfied, the radiance distribution may be the complete opposite of the one usually observed in the ocean.

IV. Dependence of Downwelling Radiance on Ocean Albedo and Atmospheric Thickness

More detailed results are given in this section in order to show the dependence of the radiation field on the ocean albedo and the atmospheric thickness. For simplicity the Rayleigh phase function was used for all scattering events in both the atmosphere and ocean in this section. In all cases the ocean-atmosphere interface reflects and refracts the light rays according to the laws of optics. No absorption is assumed in the atmosphere, unless otherwise mentioned.

The downward radiance just below the ocean surface as a function of the zenith angle of observation is shown in Fig. 2 for the case of a vanishingly small atmosphere ($\tau_{\text{atm}} = 0.0001$) and a solar zenith angle,

$\theta_0 = 11.44^\circ$. Calculations done for an atmosphere with a hundred-fold smaller thickness showed no differences on the scale of these figures. The four curves are for ocean albedo values of $\omega_0 = 1, 0.9, 0.5, 0.1$. The diffuse radiance shown here is for photons that have undergone one or more scattering events; thus the direct solar beam is not shown. In all cases the radiance increases from the zenith toward the critical angle and then exhibits only a slight variation from the critical angle to the horizon. The upwelling radiance is nearly constant. The downwelling radiance necessarily has the same variation with angle as the upwelling in the region from the critical angle to the horizon, since it is derived by total internal reflection from the upwelling in this region. The downwelling radiance at angles less than the critical angle agrees with the upwelling radiance at the same angle times the reflectance at the surface appropriate for that angle. There is essentially no incoming sky radiation from this very thin atmosphere.

How do these curves change as the atmosphere becomes thicker? The curves for $\tau_{\text{atm}} = 0.01$ are given in Fig. 3, for $\omega_0 = 1, 0.999, 0.99, 0.9, 0.5, 0.1$. The curves are essentially unchanged at angles greater than the critical angle from Fig. 2. However, the downward radiance is appreciably greater in all cases for angles less than the critical angle. This atmosphere is thick enough to develop some sky radiation which enters the ocean at all angles less than the critical angle. This sky radiation is more important when the ocean albedo is small, since the upwelling radiance in the ocean is smaller in this case also. It is interesting that a spike develops in the radiance at the critical

angle when $\omega_0 = 0.1$. The maximum sky radiance develops near the horizon in this thin atmosphere and upon entering the water, it is refracted into a narrow range of angles around the critical angle.

Curves for $\tau_{\text{atm}} = 0.5$ (corresponding approximately to our atmosphere in the visible) are given in Fig. 4. The upper set is for a solar zenith angle $\theta_0 = 11.44^\circ$, while the lower set is for $\theta_0 = 88.86^\circ$. In each case curves are shown for $\omega_0 = 1, 0.9, 0.7, 0.5, 0.1$. When $\omega_0 < 0.8$ (as is the case for the actual ocean), these curves have the typical shape observed with the largest radiance value within the critical cone. When $\omega_0 = 1$ and $\theta_0 = 11.44^\circ$, the radiance is lower within the critical cone than it is outside. When there is no absorption in the ocean, the upwelling radiation is relatively large and there is not enough sky radiation, even with this atmospheric thickness, to make the downwelling radiance larger within the critical cone than it is outside.

It is interesting to compare the lower set of five curves for $\theta_0 = 88.86^\circ$ with the upper set for $\theta_0 = 11.44^\circ$. In all cases there is a greater drop in the radiance value as θ passes through the critical angle when the sun is near the horizon than when it is near the zenith. Even when $\omega_0 = 1$ there is a maximum in the radiance curve just before the critical angle when the sun is near the horizon. These changes occur because there is relatively more sky radiation compared to the upwelling radiation in the ocean when the sun is near the horizon.

Similar curves are given in Fig. 5 for a relatively thick atmosphere, $\tau_{\text{atm}} = 5$. The downwelling radiance just below the ocean surface is nearly constant when $\omega_0 = 1$. The atmosphere is so thick that the

radiance is nearly constant above the ocean surface. Since there is no absorption within the ocean, this nearly constant radiance distribution holds down to great depths until it is eventually influenced by the nature of the bottom surface of the ocean.

For other values of the ocean albedo the downwelling radiance just below the ocean surface has a maximum at the zenith and decreases appreciably in value near the critical angle.

The model used for all the previous results has no absorption in the atmosphere. It is an interesting theoretical question to ask how a water surface changes the radiance distribution in an otherwise homogeneous medium. The curves in Fig. 6 were calculated assuming that $\omega_0(\text{atm}) = \omega_0(\text{ocean})$, i.e. the medium above and below the interface has the same properties. The optical depth of the interface is at $\tau_i = 0.5$, and $\theta_0 = 11.44^\circ$ and 88.86° . A comparison of this figure with Fig. 4 shows a much larger variation in the radiance near the critical angle in Fig. 4 than in Fig. 6 for a case such as $\omega_0 = 0.1$ and $\theta_0 = 11.44^\circ$. This is caused by the much smaller contribution of the sky radiation when $\omega_0(\text{atm}) = 0.1$ than when it is unity. The shape of the curves is much more nearly similar when Figs. 4 and 6 are compared for the cases with $\theta_0 = 88.86^\circ$. We shall return to the question of the influence of the interface in the next section.

The results of this section show that the observed decrease in the downwelling radiance just below the ocean surface as the angle of observation increases through the critical angle only occurs when there is an appropriate balance between several factors: 1. the optical

thickness of the atmosphere must be large enough to create multiple scattered sky radiation at all viewing angles; 2. the single scattering albedo of the water must be relatively small ($\omega_0 < 0.7$ approximately) so that the upwelling radiance just below the ocean surface is a small fraction of the downwelling radiance entering the ocean.

V. Dependence of Radiance on Depth in Medium

The interface between the atmosphere and ocean causes important changes in the variation of radiance with zenith angle, especially near the interface. In this section various examples are presented which illustrate how the radiance distribution varies with depth.

In order to study the change in shape of the radiance curves with optical depth, it is convenient to plot the diffuse downward radiance at a particular value of τ divided by the diffuse downward irradiance for the same value of τ . When this is done, it is possible to observe conveniently the change in shape of the curve on one graph; otherwise the simple radiance curves are eventually dominated by the exponential decrease of the radiation and are difficult to plot on a single graph. In all figures in this section the radiance has been divided by the diffuse irradiance at that optical depth. In order to save words we refer to plots of the "radiance ratio" understanding that the ratio defined above is the actual quantity plotted.

The downward radiance ratio is shown in Fig. 7 when the sun is near the horizon, $\theta_0 = 88.86^\circ$, the ocean-atmosphere interface is at an optical depth $\tau_i = 0.5$, $\omega_0(\text{atm}) = 1$, $\omega_0(\text{ocean}) = 0.5$. Near the top of the atmosphere the radiance increases toward the horizon and may reach a maximum value near the horizon as seen in the curves for $\tau = 0.1$ and 0.5 (just

above interface). The solid curve shows the downward radiance just below the interface with the typical shape increasing from the zenith to near the critical angle and then decreasing by an order of magnitude with a slow increase to the horizon. The sudden decrease near the critical angle gradually disappears with depth, but is still quite evident at $\tau = 1.5$ (as measured from the top of the atmosphere). This feature has disappeared when $\tau = 10.5$. At a depth of $\tau = 50.5$ the radiance ratio has approached the asymptotic radiance distribution closely, at least as far as can be seen on the scale of this figure. This radiance ratio distribution at great depths is identical to the one obtained for a homogeneous medium, as the interface no longer has any influence at such depths.

Only one parameter is changed in Fig. 8; the single scattering albedo in the ocean, $\omega_0(\text{ocean}) = 0.1$. The radiance ratio is nearly the same in the atmosphere at optical depths down to the interface. The radiance ratio just below the interface (solid curve) has a sharp drop of over two orders of magnitude as it passes through the critical angle. This drop is still quite evident at $\tau = 1.5$, but is beginning to disappear at $\tau = 5.5$. At still larger optical depths the radiance ratio approaches its asymptotic form; it is interesting to note that there are still noticeable differences between the actual radiance distribution at $\tau = 100.5$ and the asymptotic distribution. When $\omega_0 = 0.1$, extremely large optical depths are required to establish the asymptotic distribution.⁸

The remaining figures in this section, Figs. 9 - 12, are for the sun near the zenith, $\theta_0 = 11.44^\circ$. Each figure has an upper and lower

set of curves. The upper set is for a homogeneous medium with the indicated single scattering albedo. The lower set is for a medium with an atmosphere-ocean interface with the appropriate reflection and refraction properties for an upper medium with an index of refraction, $n = 1$, and the lower medium with $n = 1.338$. We are interested in studying the effect on the radiance distribution of the introduction of such an interface into a homogeneous medium; thus in each case the single scattering albedo in the upper medium is taken as equal to that in the lower. In all these figures the interface is taken at $\tau_i = 0.5$.

In Fig. 9, $\omega_0 = 0.99$. The downward radiance ratio has a maximum at the horizon for small optical depths. This changes into a distribution with a maximum at the zenith as τ increases. The asymptotic distribution is reached on the scale of this figure at $\tau = 5$. The radiance ratio at intermediate optical depths is quite different for the two cases with and without an interface. When an interface is present, the radiance ratio just below the interface rises toward the critical angle and then shows only a slight increase from the critical angle to the horizon. This increase still occurs at $\tau = 1.5$, but the asymptotic distribution is reached at $\tau = 5.5$, the same distribution as for the homogeneous medium without interface.

The curves in Figs. 10 and 11 are for the same parameters except that $\omega_0 = 0.5$ and 0.1 respectively. The radiance ratio at $\tau = 50$ is still somewhat different from the asymptotic distribution for $\omega_0 = 0.5$. When $\omega_0 = 0.1$, the radiance ratio at $\tau = 50$ still differs from the asymptotic distribution by factors of more than three at many angles.

This illustrates the general fact that the asymptotic distribution is valid only at increasing optical depths as ω_0 becomes smaller⁸.

The radiance just below the interface for both $\omega_0 = 0.5$ and 0.1 increases from the zenith toward the critical angle, then decreases rapidly through the critical angle, and finally increases slowly toward the horizon. When $\tau \geq 2.5$, the radiance ratio is a monotonically decreasing function of zenith angle.

In general the shape of the downward radiance ratio curves from the top of the atmosphere to the top of the interface is only slightly influenced by whether an interface is present. The downward radiance ratio at optical depths just below the interface is naturally influenced by whether or not an interface is present. This influence decreases as τ increases and has nearly vanished in all cases when $\tau = 5$.

A similar set of curves for the upward radiance ratio is given in Fig. 12 when $\omega_0 = 0.5$. With the interface at $\tau_i = 0.5$, it has little influence on the shape of the upward radiance curves when $\tau > 0.5$. However the curves for the two cases with and without the interface are quite different at optical depths such that $\tau < 0.5$. At the top of the atmosphere the upward radiance ratio is much stronger at the horizon and considerably weaker at the nadir than when the interface is present. This is due to two factors: the stronger reflection of the direct beam from the interface for angles near the horizon than for those near the nadir and the fact that the interface prevents an appreciable fraction of the upwelling light from optical depths $\tau > 0.5$ from escaping through the interface.

VI. Dependence of Radiance on Position of Interface

The variation of the radiance with the position of the atmosphere-ocean interface is illustrated by the Figs. 13-18. The radiance just below and just above the interface is given in Figs. 13-14 when $\omega_0(\text{atm}) = 1$ and $\omega_0(\text{ocean}) = 0.5$. The solar zenith angle is 11.44° . When the optical depth of the interface is small ($\tau_i = 10^{-6}$), the downward radiance increases from a very small (0.0054) value at the zenith to a value almost two orders of magnitude larger near the critical angle; it is then much more nearly constant to the horizon. The upward radiance necessarily has the same value as the downward at angles greater than the critical angle (because when it is totally internally reflected it becomes the downward radiance at these angles); the upward radiance only shows minor variations from the nadir to the critical angle. As τ_i increases, there is the same qualitative variation of the radiance for $\tau_i = 0.01$, but when $\tau_i = 0.5$, the incoming radiation from the sky has become large enough to make the downward radiance just below the surface larger for angles within the critical angle than without.

These results may be compared with the downward and upward radiance just above the surface as shown in Fig. 14. The downward radiance (sky radiation) just above the interface increases uniformly from the zenith to the horizon for $\tau_i = 10^{-6}$ and 10^{-2} . When $\tau_i = 0.5$ and 1 it has a maximum near the horizon, while it decreases from the zenith to the horizon when $\tau_i = 5$. On the other hand, the upward radiance just above the interface increases from the nadir to the horizon for $\tau_i = 10^{-6}$ and 10^{-2} , but when $\tau_i = 0.5$ it passes through a minimum near 83° and then

increases to the horizon. This increase near the horizon is caused by the strong reflection of the downward radiance by the interface for incident angles near 90° . When $\tau_i = 1$ and 5, the upward radiance just above the interface again increases uniformly from the nadir to the horizon. Of course the upward and downward radiances must have the same value at the horizon.

In order to determine how the radiance varies with solar angle, the downward and upward radiance just below the surface are shown in Fig. 15 for the same parameters as in the last two figures, except that $\theta_0 = 88.86^{\circ}$. It is interesting to observe that, when τ_i has the very small value 10^{-4} , the downward radiance has a sharp maximum near the critical angle; when $\tau_i = 10^{-2}$, it increases to a maximum near the critical angle that is about eight times greater than its value at the zenith. This variation develops at much smaller optical depths when the sun is near the horizon than when it is near the zenith due to the much greater thickness traversed by the direct solar beam in the former case.

The somewhat complicated interrelationships between the different components of the radiance just above and just below the interface are illustrated in Figs. 16, 17 and 18 for models with $\omega_0(\text{atm}) = \omega_0(\text{ocean}) = 0.5, 0.9$ and 0.1 respectively. The interface is taken at $\tau_i = 0.5$. In these figures the upward and downward radiance is shown both just above and below the interface. In addition, the downward radiance just above the interface is shown multiplied by the reflection between air and water, $R(A, W)$, (this component becomes part of the upward radiance just above the interface), and multiplied by the transmission of the interface going from air to water, $T(A, W)$ (this becomes part of the downward radiance

just below the interface). In the latter case it is plotted as this part of the radiance would appear in the water after passing through the interface. This shows that the reflected downward radiance makes a major contribution to the upward radiance just above the interface only at angles near the horizon, because the reflectivity of water is near unity only at such angles. Similarly the downward radiance transmitted through the interface is the major component of the downward radiance just below the interface for angles from the zenith to those quite near the critical angle. Of course it can make no contribution at angles greater than the critical angle.

Also in this figure the upward radiance just below the interface is shown multiplied by the reflection between water and air, $R(W, A)$ (this component becomes part of the downward radiance just below the interface), and multiplied by the transmission of the interface going from water to air, $T(W, A)$ (this becomes part of the upward radiance just above the interface). This is plotted as this part of the radiance would appear in the atmosphere after passing through the interface. The reflected upward radiance just below the interface becomes the entire downward radiance just below the interface at angles greater than the critical angle, but is a major part of the downward radiance only over a small additional range of angles slightly smaller than the critical angle. The transmitted upward radiance that passes through the interface is the major component of the upward radiance above the interface from the nadir to angles relatively near the horizon.

The large variation in the shape of the curve representing the downward radiance just below the interface as ω_0 and τ_i vary is illu-

strated in Fig. 19. The ratio of the downward radiance at 8.52° to that at 49.37° is shown as a function of ω_0 . The first angle chosen is the quadrature point nearest the zenith, while the second is the first quadrature point past the critical angle. Thus this ratio indicates whether the radiance near the zenith is greater than or less than the radiance just beyond the critical angle. When $\theta_0 = 11.46^\circ$ and $\tau_i = 0.0001$, this ratio is of the order of 0.02, but as the interface is moved down, the ratio rapidly increases. When $\tau_i = 5$, this ratio is greater than 100 when $\omega_0 = 0.1$, indicating that the radiance is much larger near the zenith than at the horizon, and that it drops appreciably near the critical angle.

In Fig. 20 the ratio plotted is that of the maximum value of the downward radiance just below the interface to the value at 49.37° . These curves indicate that this ratio increases as τ_i and θ_0 increase and ω_0 decreases.

VII. Vector and Scalar Irradiance

The vector irradiance or flux, H , is defined as the integral of the product of the radiance with the cosine of the angle of observation. The upward vector irradiance, H_u , is obtained by performing the integral over all angles for the upward hemisphere; the downward vector irradiance, H_d , is obtained from the integral over the downward hemisphere. The total vector irradiance is the integral over all solid angles and equals $H_u - H_d$. The scalar irradiance, h , is the integral of the radiance over solid angle (upward hemisphere, downward hemisphere, or all solid angles).

The reflectance at a given depth in the medium is defined as $R = H_u/H_d$, while the distribution function $D = h/H$ (defined for either downward or upward irradiances). These quantities provide a relatively simple description of the variation of the radiation with depth in the medium without the additional complexity of having to specify in detail the variation of the radiance with angle.

In Table I the total upward irradiance including the direct solar beam reflected from the water interface is tabulated in the second and third columns as a function of the optical depth from the top of the medium. The values in these tables are for $\theta_0 = 11.44^\circ$ and $\omega_0 = 0.5$ or 0.1 . The values in the columns marked "homog." are for a homogeneous medium with these properties and no interface. When an interface is present, $\omega_0(\text{atm}) = \omega_0(\text{ocean}) = 0.5$ or 0.1 . The values in the columns marked "with interface" have an atmosphere-water interface at an optical depth of 0.5 . Thus a comparison of these two columns shows directly the influence of the interface.

When $\omega_0 = 0.5$ the upward irradiance is smaller above the interface ($\tau < 0.5$) in the medium with the interface than at comparable depths in the homogeneous medium, while it is greater at corresponding depths in the medium with the interface when $\tau > 0.5$. This variation is in the opposite sense when $\omega_0 = 0.1$. In the latter case there is so much absorption in the medium that the radiation from the direct beam reflected into the upward direction at the interface makes an appreciable contribution to the irradiance when $\tau < 0.5$. On the other hand when there is less absorption, $\omega_0 = 0.5$, the upward irradiance is much larger at all levels

compared to the case with $\omega_0 = 0.1$. Only part of the upward irradiance just below the interface is transmitted through the interface, with the result that the total upward irradiance is less when $\tau < 0.5$ for the medium with the interface than for the homogeneous medium. The reflected solar beam makes only a minor contribution to the total upward irradiance above the interface when $\omega_0 = 0.5$.

The fourth and fifth columns in Table I give the total downward irradiance including the direct solar beam for these two media. In this study the downward flux is always normalized to unity for a plane perpendicular to the incoming beam. When $\omega_0 = 0.5$, the downward irradiance is greater just below the interface than it is in the homogeneous medium at the same depth due to the upwelling radiation reflected into the downward direction by the interface. The opposite situation prevails when $\omega_0 = 0.1$, since the upwelling irradiance is so small; in this case the loss of some of the downward irradiance by reflection at the interface is the determining factor in this variation.

The last two columns give the total scalar irradiance ($h_u + h_d$) which is proportional to the heating rate at the given depth. This quantity is less for the medium with the interface than for the homogeneous medium when $\tau < 0.5$ and $\omega_0 = 0.5$, while it is larger when $\tau > 0.5$. There is the opposite variation when $\omega_0 = 0.1$. All of the quantities in Table I decrease nearly exponentially with optical depth when measured reasonably far from boundaries.

On the other hand the quantities in Table II are remarkably constant throughout the medium. The second and third columns of Table II give the reflectance. The fourth and fifth columns give the ratio of the total upward irradiance to the total downward irradiance (total means that

the direct beam is included in the downward irradiance and that the reflected direct beam from the interface is included in the upward irradiance; diffuse means that these quantities are not included).

The distribution function $D_u = h_u/H_u$ is given in the sixth and seventh columns. In this expression H_u and h_u are the total upward irradiance and total upward scalar irradiance respectively, including the contribution from the solar beam reflected at the interface. The eighth and ninth columns give the same quantity for the downward radiation, $D_d = h_d/H_d$, with the use of the total irradiance and scalar irradiance, including the contribution from the solar beam. The last two columns give the distribution function for the downward radiation, but only the diffuse contribution to the irradiance and scalar irradiance is used.

The distribution function is important because it depends on the variation of the radiance with angle. If the radiation is monodirectional with direction cosine μ_0 , then $D = 1/\mu_0$, while if the radiance is uniformly distributed with angle, then $D = 2$. If D is close to unity, the radiance has a maximum near the zenith (for downwelling radiation) and only small values near the horizon. Similarly if $D > 2$, the radiance is greater near the horizon than near the zenith. Thus in the last column of Table II, $D = 2.943$ in the medium with an interface, when $\tau = 0.1$ and $\omega_0 = 0.5$, since the diffuse radiation develops first near the horizon at small optical depths because of the greater effective optical thickness there. Note the different values of D just above and just below the interface. Just below the interface, $D = 1.863$, since the downwelling radiation is largely confined within the critical cone around the zenith direction. At great depths $D = 1.359$ corresponding to the radiance distribution peaked around the zenith that develops in the diffusion region in an absorbing medium.

The variation of some of these quantities is shown in Fig. 21 for the case $\theta_0 = 11.44^\circ$, $\tau_i = 0.5$, $\omega_0(\text{atm}) = 1$, $\omega_0(\text{ocean}) = 0.5$. The following quantities are indicated as a function of the optical depth from the top of the atmosphere: total and diffuse upward and irradiance, total and diffuse downward irradiance, the net flux equal to the difference between the total downward and total upward irradiances, and the derivative with respect to optical depth of the total flux (which is proportional to the heating rate).

Under what conditions does the diffuse flux increase or decrease upon passing through the interface? This is illustrated in Table III which gives the ratio of the downward diffuse irradiance (direct solar beam not included) just below the interface to that just above; the same ratio for the upward diffuse irradiance (direct solar beam reflected by interface not included) is also shown. In most cases given in the Table, the downward diffuse irradiance is greater just below the interface than above. In some cases it is two to three orders of magnitude greater, e.g. when the interface is near the top of the atmosphere and the sun is near the zenith. In these cases there is insufficient atmosphere for any appreciable downwelling scattered radiation to develop. The downward diffuse radiance just below the interface is less than that just above only in cases where the absorption in the ocean is appreciable and the interface is at an intermediate optical depth. When the ocean absorption is large, there is a much smaller upwelling irradiance in the ocean and thus relatively little radiation is reflected at the interface into the downward direction. The ratios for the upward irradiance can be explained in a similar manner.

VIII. Effect of Phase Function

All results given in the previous sections assume a Rayleigh phase function for the scattering centers in both the atmosphere and ocean. It is realized, of course, that the results would be changed for other phase functions. In order to explore how large the changes are that might be anticipated, some of the calculations were repeated with a more realistic phase function in the ocean. The phase function chosen was proportional to $A(\mu + 0.75)^{32} + B$, where $A = 2.52 \times 10^{-7}$, $B = 0.1$, and μ is the cosine of the scattering angle. The ratio of scattering into the forward hemisphere to that into the backward is 9, while the ratio of the scattering at 0° to that at 180° is 152. The form of this function was chosen merely because it could be included in the computer program with relative ease. However, it does reproduce some of the features of a realistic ocean phase function, such as a strong forward to backward scattering ratio and a peak around 0° .

The downward and upward radiance just below the interface is shown in Fig. 22. In order to study the transition from Rayleigh to a Mie-type phase function, calculations were made for several values of the parameter $\beta = \sigma_{SR}/\sigma_{ST}$, where σ_{SR} is the scattering cross section in the ocean for Rayleigh scattering processes and σ_{ST} is the total scattering cross section from all processes. Thus when $\beta = 1$, the scattering is entirely Rayleigh and the results are the same as those given in the previous sections. When $\beta = 0$, there is not Rayleigh scattering and all scattering is by the phase function given in the previous paragraph.

The upwelling radiance shown in Fig. 22 shows that this quantity decreases appreciably as the scattering becomes predominately in the forward direction, since the downwelling photons have less chance to be scattered

into an upward direction. This has relatively little effect on the downwelling radiance within the critical cone. However the effect is large outside the critical cone, since the downwelling radiance in this range of angles is entirely derived from the upwelling radiance totally internally reflected at the atmosphere-water interface.

IX. Conclusion

The influence of the various properties of an atmosphere-ocean system on the radiance distribution has been explored. The downwelling radiance just below the ocean surface has a well-known maximum within the cone extending out to the critical angle and then decreases by one to two orders of magnitude toward the horizon. This observed variation in the visible in actual bodies of water depends not only on the laws of reflection and refraction at the interface, but crucially on two other properties of the medium. The atmosphere must have sufficient optical depth to develop enough multiple scattered sky radiation at all angles to provide the source for the enhanced light observed within the critical angle just beneath the ocean surface. In addition the water must have a fairly high absorption for visible light, so that the ratio of the upwelling to downwelling light within the ocean is small. When this happens the downwelling light outside the critical angle just beneath the ocean surface (derived by total internal reflection from the weak upwelling light) is one or two orders of magnitude less than the downwelling light within the critical angle. Numerous examples given here show that just the opposite situation occurs when these conditions are not satisfied.

The radiance distribution with depth for a homogeneous medium is compared with that for an identical medium, but with an atmosphere-ocean interface. The influence of the interface on the radiance, irradiance, heating rate and many other properties of the radiation has been illustrated. The variation of these quantities with depth is complex in its dependence on the scattering and absorption properties of the atmosphere and ocean, including the phase function for scattering as well as the optical depth from the top of the atmosphere of the atmosphere-ocean interface.

References

1. G. N. Plass, G. W. Kattawar and F. E. Catchings, Appl. Opt. 12, 314 (1973).
2. G. W. Kattawar, G. N. Plass and F. E. Catchings, Appl. Opt. 12, 1071 (1973).
3. G. W. Kattawar, G. N. Plass and S. J. Hitzfelder, Appl. Opt. 15, 632 (1976).
4. G. W. Kattawar, T. J. Humphreys and G. N. Plass, SPIE Ocean Optics V, 160, 123 (1978).
5. J. Potter, Jr., J. Atmosph. Sci., 27, 943 (1970).
6. A. Gershun, J. Math. and Phys. 18, 53 (1939).
7. G. N. Plass, G. W. Kattawar and S. J. Hitzfelder, Appl. Opt. 15, 1003 (1976).
8. G. W. Kattawar and G. N. Plass, Appl. Opt. 15, 3166 (1976).
9. G. N. Plass, T. J. Humphreys and G. W. Kattawar, Appl. Opt. 17, 1432 (1978).
10. G. N. Plass, G. W. Kattawar and J. A. Guinn, Jr., Appl. Opt. 14, 1924 (1975).
11. G. N. Plass and G. W. Kattawar, J. Phys. Oceanogr. 2, 139 (1972).
12. G. W. Kattawar and G. N. Plass, J. Phys. Oceanogr. 2, 146 (1972).

TABLE I

$$\omega_0 = 0.5 ; \theta_0 = 11.44^\circ$$

τ	$H_u(\text{total})$		$H_d(\text{total})$		$h_u + h_d$	
	homog.	with interface	homog.	with interface	homog.	with interface
0	0.1192	0.1094	0.9801	.9801	1.240	1.220
.1	.1118	.1004	.9113	.9108	1.207	1.182
.5*	8.346-2***	6.255-2	.6673	.6647	0.9442	0.8894
.5**	8.346-2	8.598-2	.6673	.6882	.9442	.9682
1	5.604-2	5.784-2	.4422	.4565	.6494	.6701
2	2.411-2	2.480-2	.1876	.1932	.2859	.2935
5	1.665-3	1.717-3	1.274-2	1.317-2	2.021-2	2.080-2
10	1.665-5	1.734-5	1.256-4	1.318-4	2.033-4	2.127-4
20	1.395-9	1.494-9	1.054-8	1.129-8	1.724-8	1.844-8
50	6.638-22	7.238-22	5.006-21	5.458-21	8.224-21	8.966-21

$$\omega_0 = 0.1 ; \theta_0 = 11.44^\circ$$

0	1.754-2	2.304-2	0.9801	0.9801	1.035	1.040
.1	1.594-2	2.191-2	.8893	.8893	0.9457	0.9523
.5*	1.080-2	1.886-2	.6003	.6004	.6467	.6524
.5**	1.080-2	1.061-2	.6003	.5921	.6467	.6317
1	6.591-3	6.510-3	.3657	.3623	.3967	.3898
2	2.436-3	2.424-3	.1349	.1346	.1472	.1457
5	1.200-4	1.220-4	6.627-3	6.755-3	7.282-3	7.368-3
10	7.738-7	8.143-7	4.269-5	4.503-5	4.704-5	4.931-5
20	3.153-11	3.511-11	1.739-9	1.939-9	1.918-9	2.129-9
50	4.776-26	2.630-24	1.205-22	1.452-22	1.013-22	1.597-22

*above interface
 **below interface
 ***represents 8.346×10^{-2}

TABLE II

$\omega_0 = 0.5 ; \theta_0 = 11.44^\circ$

R	$h_u(\text{total})/h_d(\text{total})$		$h_u(\text{total})/H_u(\text{total})$		$h_d(\text{total})/H_d(\text{total})$		$h_d(\text{dif.})/H_d(\text{dif.})$	
	homog.	with interface	homog.	with interface	homog.	with interface	homog.	with interface
0	.1216	.1116	.2395	.2202	2.009	2.012	1.020	1.020
.1	.1227	.1103	.2310	.2081	2.026	2.028	1.076	1.075
.5*	.1251	.0941	.2225	.1617	2.059	1.979	1.158	1.152
.5**	.1251	.1249	.2225	.2235	2.059	2.057	1.158	1.150
1	.1267	.1267	.2187	.2187	2.080	2.079	1.205	1.204
2	.1286	.1284	.2154	.2156	2.102	2.100	1.254	1.252
5	.1307	.1306	.2123	.2124	2.128	2.127	1.309	1.308
10	.1318	.1317	.2109	.2111	2.140	2.139	1.337	1.334
20	.1324	.1323	.2102	.2103	2.147	2.147	1.353	1.350
50	.1326	.1326	.2100	.2100	2.150	2.150	1.358	1.358
100	.1326	.1326	.2100	.2100	2.150	2.150	1.358	1.358
$\omega_0 = 0.1 ; \theta_0 = 11.44^\circ$								
0	1.790-2	2.351-2	3.516-2	4.005-2	2.005	1.739	1.020	1.020
.1	1.793-2	2.464-2	3.497-2	4.063-2	2.008	1.697	1.029	1.029
.5*	1.798-2	3.141-2	3.478-2	4.340-2	2.015	1.439	1.042	1.041
.5**	1.798-2	1.792-2	3.478-2	3.488-2	2.015	2.006	1.042	1.031
1	1.802-2	1.797-2	3.470-2	3.476-2	2.019	2.011	1.048	1.040
2	1.807-2	1.800-2	3.463-2	3.468-2	2.023	2.016	1.055	1.046
5	1.812-2	1.806-2	3.456-2	3.461-2	2.028	2.022	1.063	1.055
10	1.814-2	1.808-2	3.453-2	3.458-2	2.032	2.025	1.067	1.059
20	1.815-2	1.810-2	3.451-2	3.456-2	2.033	2.027	1.070	1.061
50	1.816-2	1.811-2	3.450-2	3.455-2	2.034	2.028	1.070	1.063

*above interface

**below interface

TABLE III

Ratio Diffuse Irradiance Just Below to Diffuse Irradiance Just Above Interface

τ_j	ω_0	Downward			Upward		
		$\theta_0=11.44^\circ$	$\theta_0=76.28^\circ$	$\theta_0=88.86^\circ$	$\theta_0=11.44^\circ$	$\theta_0=76.28^\circ$	$\theta_0=88.86^\circ$
0.0001	1	6334	2181	24.89	1.896	1.982	1.937
	0.9	3540	900.7	9.442	1.968	2.089	2.048
	0.5	1070	236.7	2.956	1.924	2.155	1.968
	0.1	155.5	33.33	1.101	1.861	2.146	1.231
0.01	1	64.28	22.83	1.796	1.893	1.939	1.649
	0.9	36.01	9.856	1.155	1.960	2.045	1.312
	0.5	11.49	3.185	0.868	1.903	1.983	0.611
	0.1	2.397	1.147	0.830	1.730	1.321	0.111
0.5	1	2.757	1.893	1.770	1.829	1.778	1.771
	0.9	1.784	1.261	1.210	1.814	1.620	1.600
	0.7	1.351	1.074	1.056	1.669	1.315	1.286
	0.5	1.155	0.999	0.995	1.472	0.992	0.964
	0.1	0.952	0.926	0.937	0.593	0.231	0.222
1	1	2.156	1.794	1.784	1.810	1.782	1.786
	0.9	1.450	1.223	1.221	1.757	1.636	1.648
	0.5	1.066	1.004	1.006	1.316	1.026	1.050
	0.1	0.950	0.943	0.948	0.434	0.248	0.260
5	1	1.794	1.788	1.788	1.792	1.791	1.790
	0.9	1.230	1.226	1.226	1.674	1.671	1.672
	0.5	1.013	1.012	1.012	1.108	1.101	1.101
	0.1	1.000	1.000	1.000	0.290	0.286	0.286

Legends for Figures

- Fig. 1. Downward radiance just below ocean surface as function of zenith angle of observation θ for solar zenith angle $\theta_0 = 11.44^\circ$. The top curve has single scattering albedo in the ocean, $\omega_0 = 0.5$ and an atmosphere of optical thickness $\tau_{atm} = 0.5$. The middle curve has $\omega_0 = 0.5$ and $\tau_{atm} = 0.0001$. The bottom curve has $\omega_0 = 1.0$ and $\tau_{atm} = 0.5$.
- Fig. 2. Downward radiance just below ocean surface as function of θ for $\theta_0 = 11.44^\circ$, $\tau_{atm} = 0.0001$ and $\omega_0 = 0.1, 0.5, 0.9, 1.0$.
- Fig. 3. Downward radiance just below ocean surface as function of θ for $\theta_0 = 11.44^\circ$, $\tau_{atm} = 0.01$ and $\omega_0 = 0.1, 0.5, 0.9, 0.99, 0.999, 1.0$.
- Fig. 4. Downward radiance just below ocean surface as function of θ for $\theta_0 = 11.44^\circ$ and 88.86° , $\tau_{atm} = 0.5$ and $\omega_0 = 0.1, 0.5, 0.7, 0.9, 1.0$.
- Fig. 5. Downward radiance just below ocean surface as function of θ for $\theta_0 = 11.44^\circ$ and 88.86° , $\tau_{atm} = 5$ and $\omega_0 = 0.1, 0.5, 0.9, 1.0$.
- Fig. 6. Downward radiance just below ocean surface as a function of θ for $\theta_0 = 11.44^\circ$ and 88.86° , $\tau_i = 0.5$, $\omega_0(atm) = \omega_0(ocean)$ and $\omega_0 = 0.1, 0.5, 0.7, 0.9, 0.99, 1.0$.
- Fig. 7. Downward radiance divided by diffuse downward scalar irradiance as a function of θ for $\theta_0 = 88.86^\circ$, $\tau_i = 0.5$, $\omega_0 = 0.5$ at various optical depths measured from top of atmosphere.

Fig. 8. Same as Fig. 7, except $\omega_0 = 0.1$.

Fig. 9. Downward radiance divided by diffuse downward irradiance as a function of θ for $\theta_0 = 11.44^\circ$ at various optical depths. The upper curves are for a homogeneous medium with $\omega_0 = 0.99$. The lower curves are for a medium with an interface at an optical depth $\tau_i = 0.5$ and with $\omega_0(\text{atm}) = \omega_0(\text{ocean}) = 0.99$.

Fig. 10. Same as Fig. 9 except $\omega_0 = 0.5$ for upper curves and $\omega_0(\text{atm}) = \omega_0(\text{ocean}) = 0.5$ for lower curves.

Fig. 11. Same as Fig. 9 except $\omega_0 = 0.1$ for upper curves and $\omega_0(\text{atm}) = \omega_0(\text{ocean}) = 0.1$ for lower curves.

Fig. 12. Upward radiance divided by upward irradiance as a function of θ for $\theta_0 = 11.44^\circ$ at various optical depths. The upper curves are for a homogeneous medium with $\omega_0 = 0.5$. The lower curves are for a medium with an interface at an optical depth $\tau_i = 0.5$ and with $\omega_0(\text{atm}) = \omega_0(\text{ocean}) = 0.5$.

Fig. 13. The upward and downward radiance (divided in both cases by downward radiance) just below the interface for $\theta_0 = 11.44^\circ$, $\omega_0(\text{atm}) = 1$, $\omega_0(\text{ocean}) = 0.5$, with the interface at the following optical depths: $\tau_i = 10^{-6}, 10^{-2}, 0.5, 1, 5$.

Fig. 14. The upward and downward radiance just above the interface for $\theta_0 = 11.44^\circ$, $\omega_0(\text{atm}) = 1$, $\omega_0(\text{ocean}) = 0.5$, with the interface at the following optical depths: $\tau_i = 10^{-6}, 10^{-4}, 10^{-2}, 0.5, 1, 5$.

Fig. 15. The upward and downward radiance just below the interface for $\theta_0 = 88.86^\circ$, $\omega_0(\text{atm}) = 1$, $\omega_0(\text{ocean}) = 0.5$, with the interface at the following optical depths: $\tau_i = 10^{-6}, 10^{-4}, 10^{-2}, 0.5, 1, 5$.

Fig. 16. The upward and downward radiance just above and just below the interface for $\theta_0 = 11.44^\circ$, $\omega_0(\text{atm}) = \omega_0(\text{ocean}) = 0.5$, and $\tau_i = 0.5$. These radiances are also shown multiplied by the reflection and transmission of the interface going from air to water, $R(A, W)$ and $T(A, W)$ respectively. They are also shown multiplied by the reflection and transmission of the interface going from water to air, $R(W, A)$ and $T(W, A)$ respectively.

Fig. 17. Same as Fig. 16 except $\omega_0(\text{atm}) = \omega_0(\text{ocean}) = 0.9$.

Fig. 18. Same as Fig. 16 except $\omega_0(\text{atm}) = \omega_0(\text{ocean}) = 0.1$.

Fig. 19. Ratio of downward diffuse radiance just below interface at 8.52° to that at 49.37° (just beyond critical angle) as a function of ω_0 for various values of τ_i and θ_0 .

Fig. 20. Ratio of maximum value of downward diffuse radiance just below interface to radiance value at 49.37° (just beyond critical angle) as a function of ω_0 for various values of τ_i and θ_0 .

Fig. 21. The total and diffuse upward irradiance, H_u , the total and diffuse downward irradiance, H_d , the total net flux, $H_d - H_u$, and the derivative of the total flux with respect to optical depth (proportional to heating rate) as a function of optical depth in the medium for $\theta_0 = 11.44^\circ$, $\tau_i = 0.5$, $\omega_0(\text{atm}) = 1$, $\omega_0(\text{ocean}) = 0.5$.

Fig. 22. The upward and downward radiance just below the interface for various values of β , the ratio of the Rayleigh scattering cross section to the total (Rayleigh plus Mie --- see text) scattering cross section.

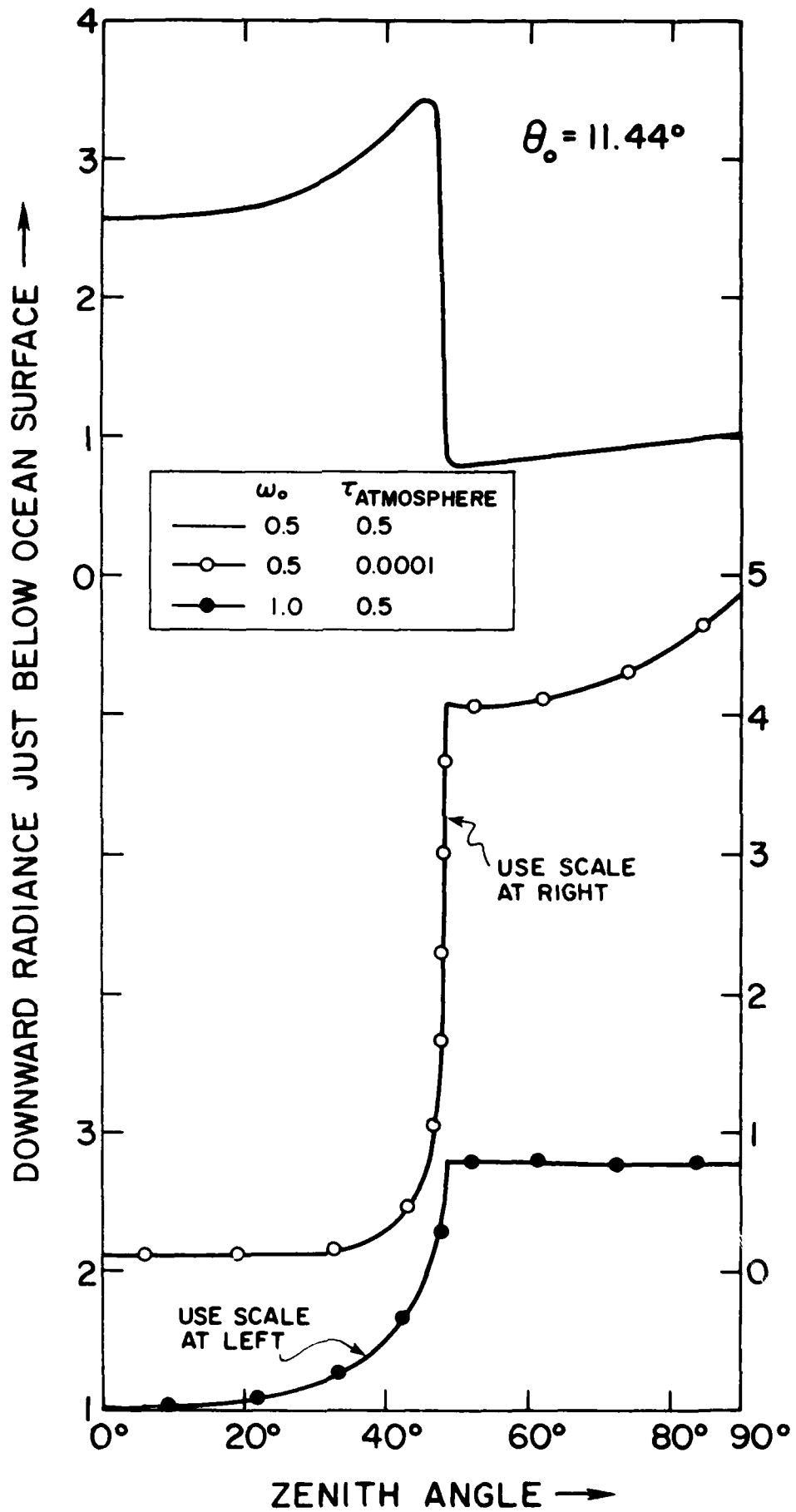


Fig. 1

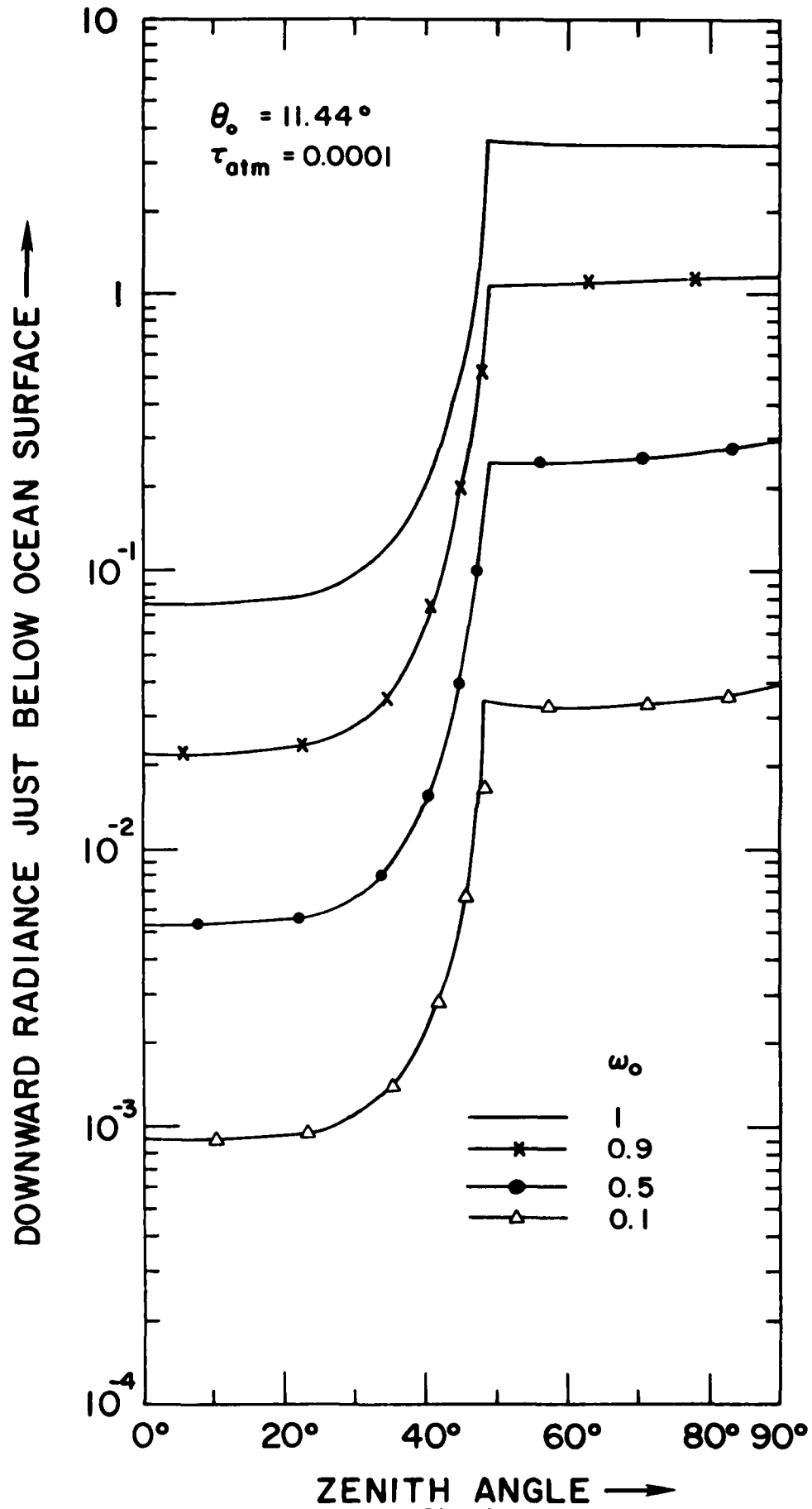


Fig. 2

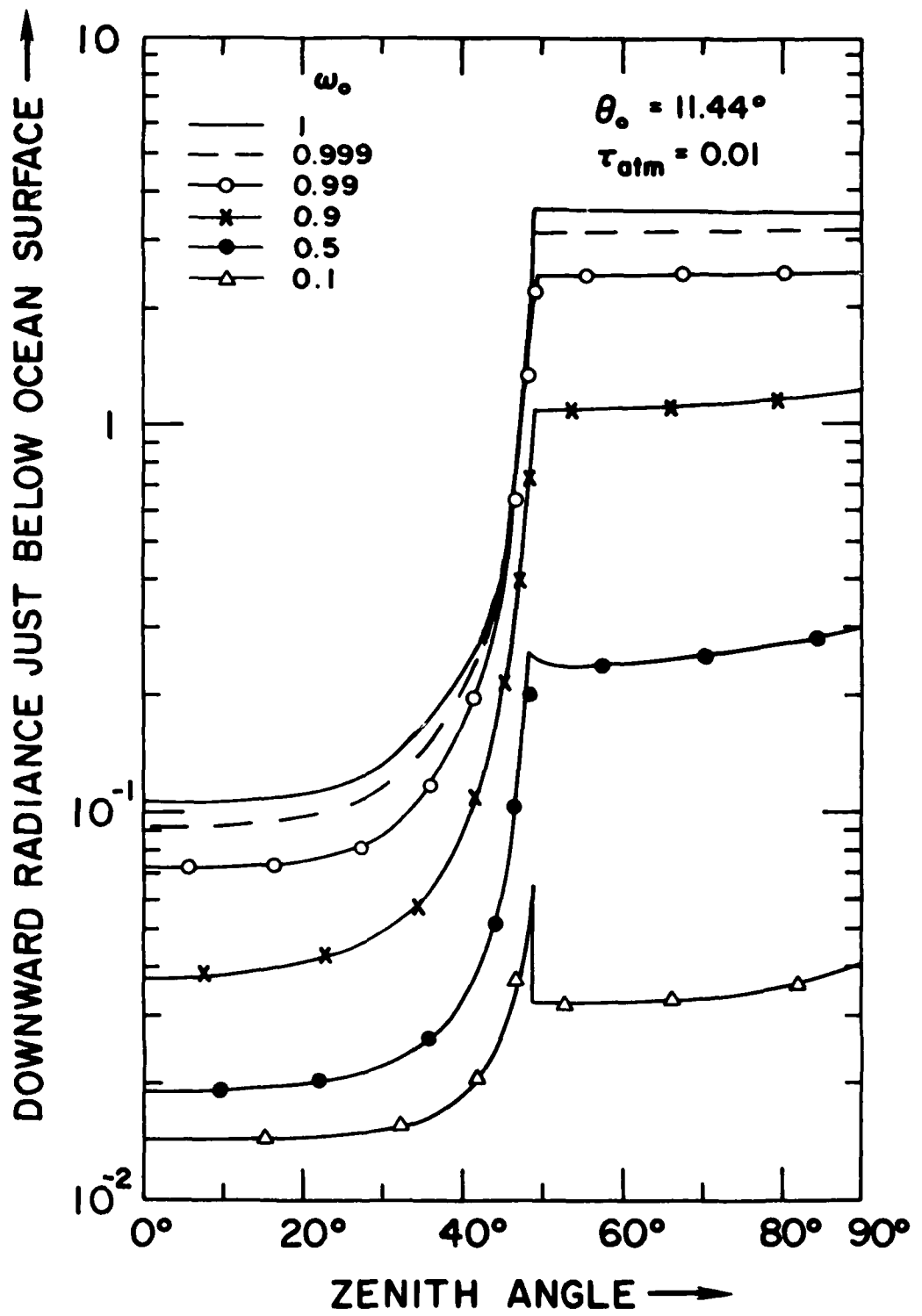


Fig. 3

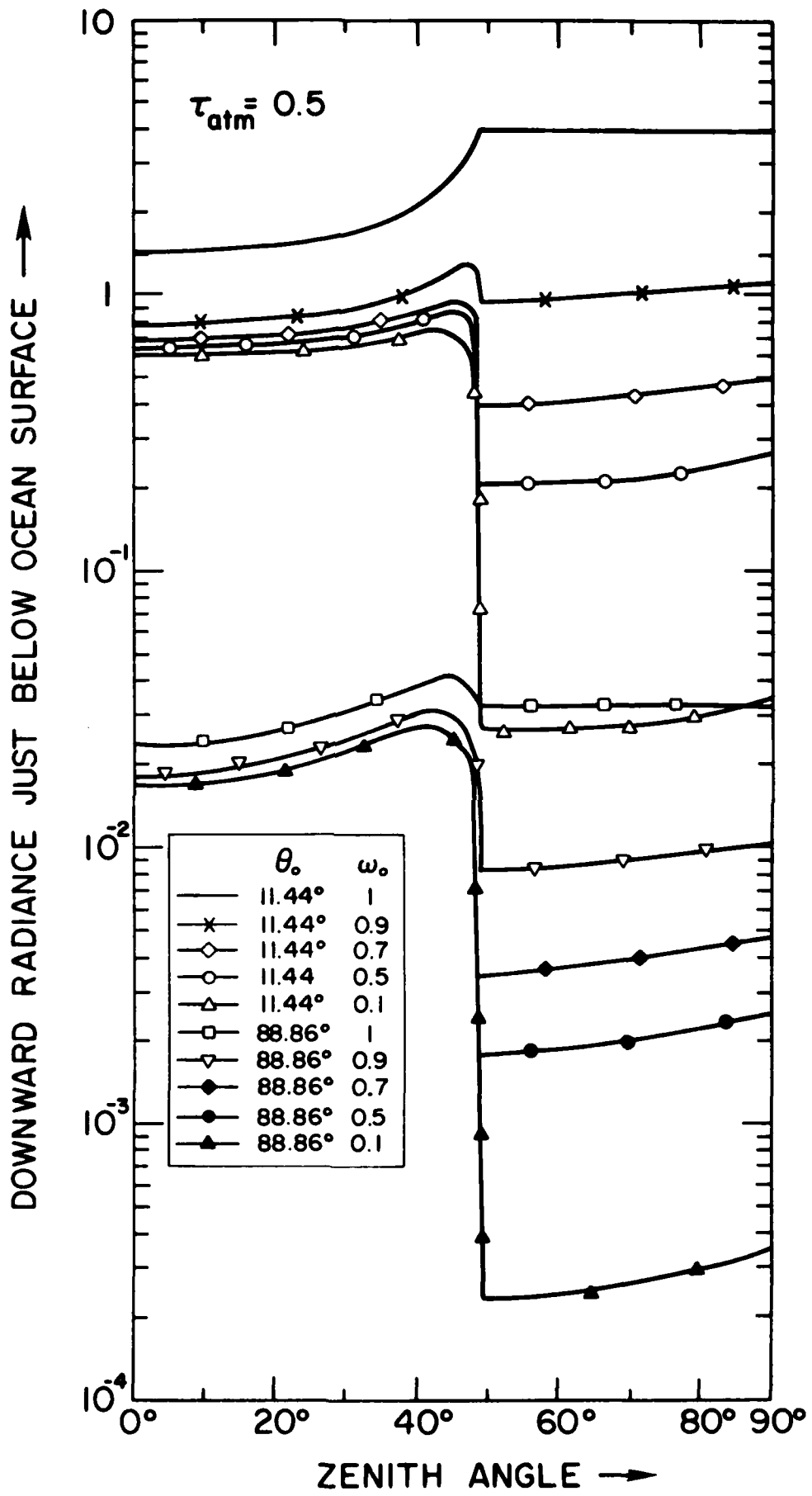


Fig. 4

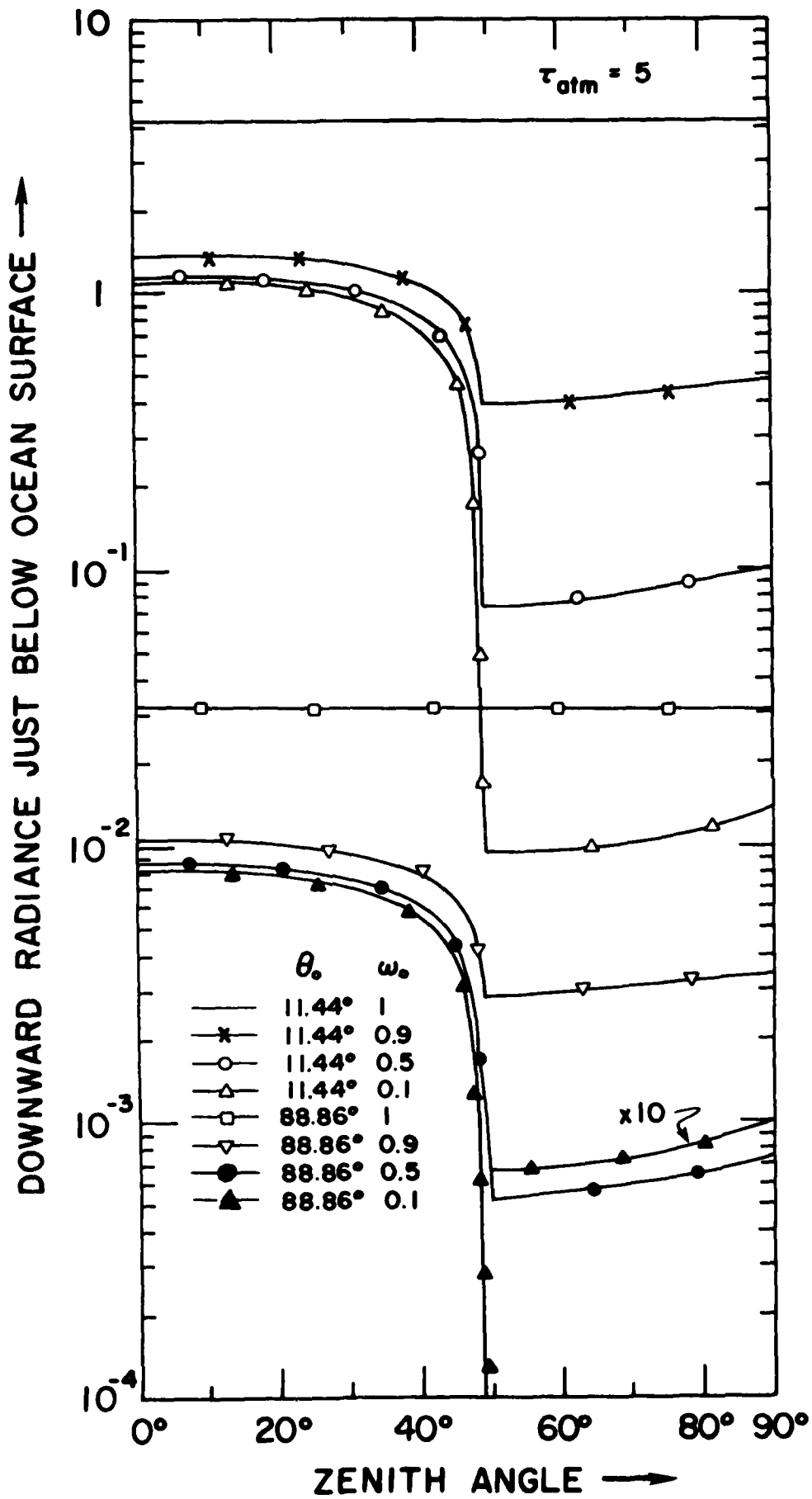


Fig. 5

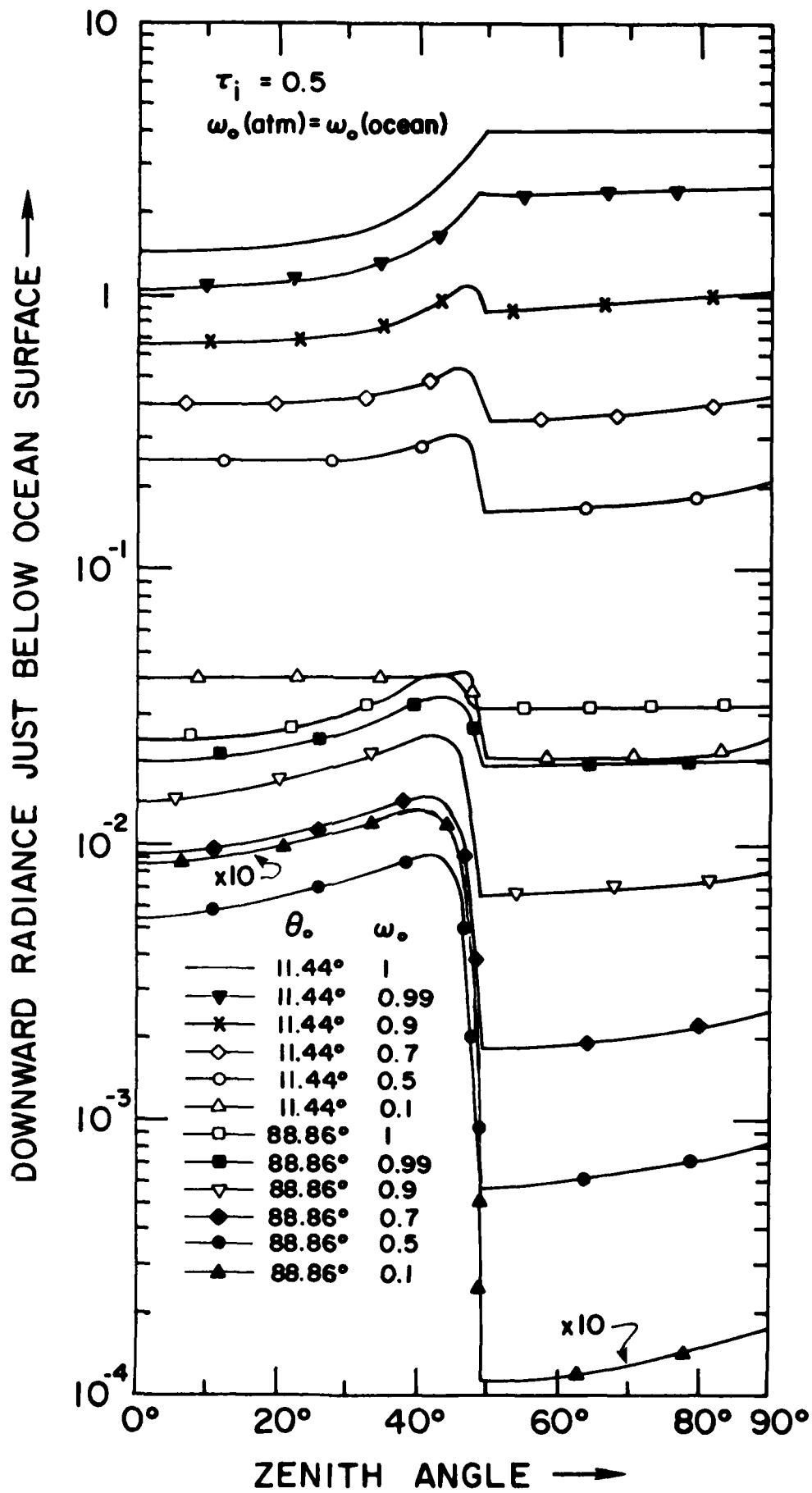


Fig. 6

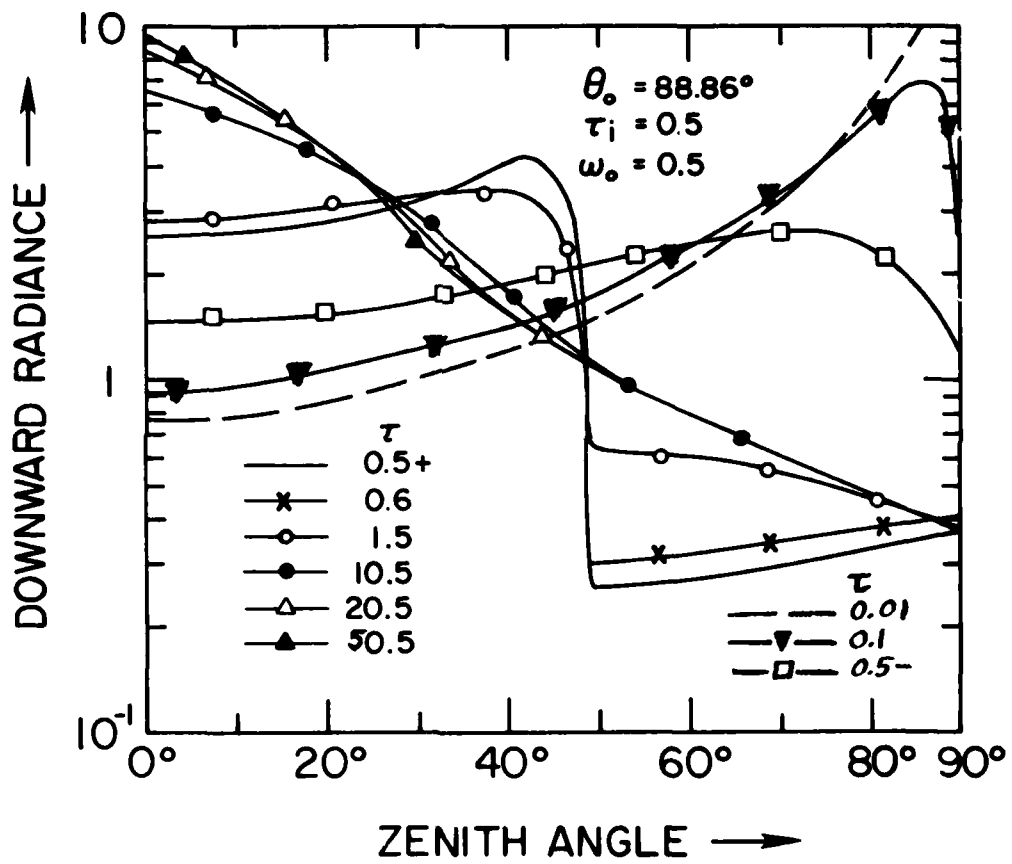


Fig. 7

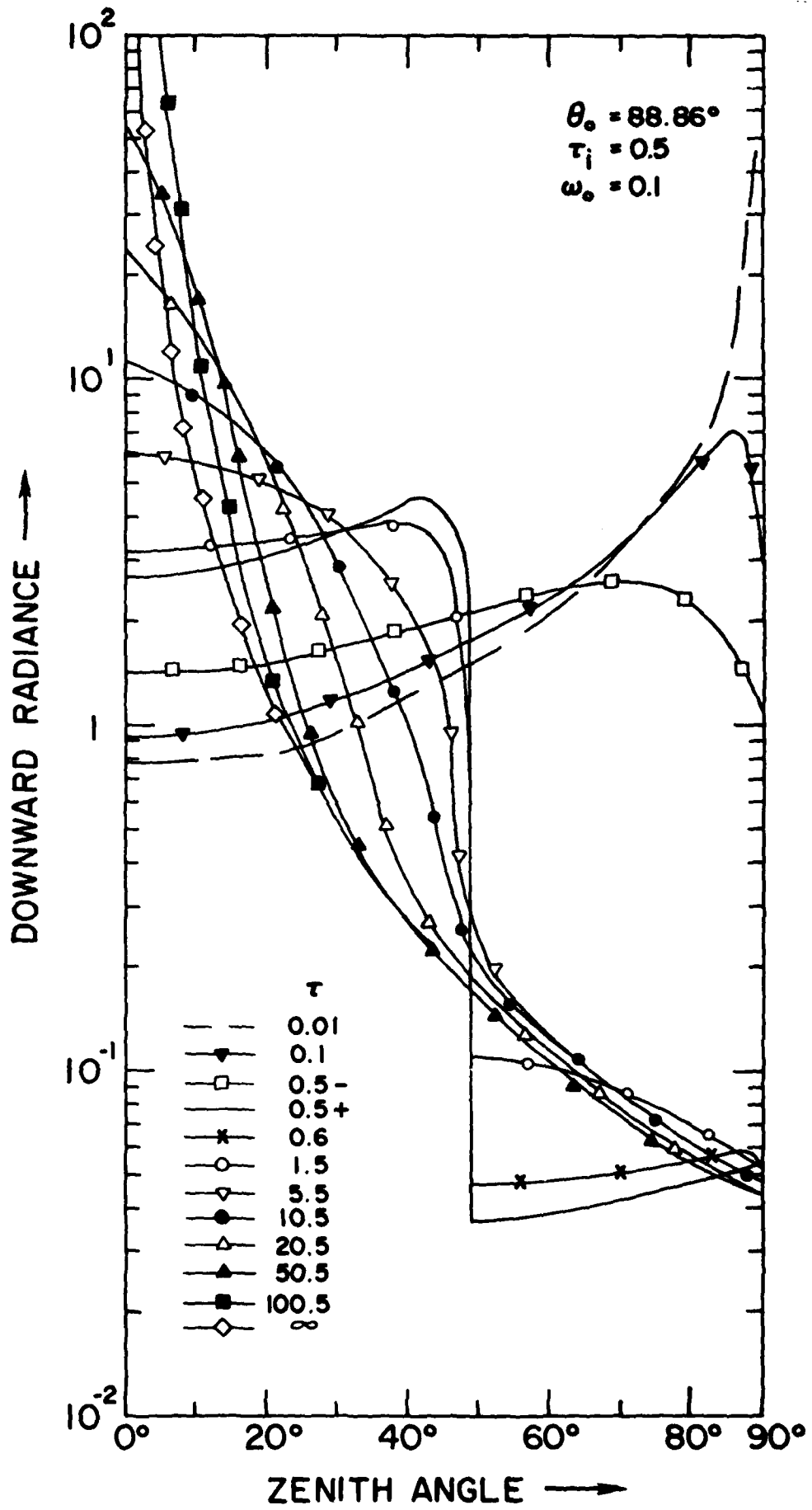


Fig. 8

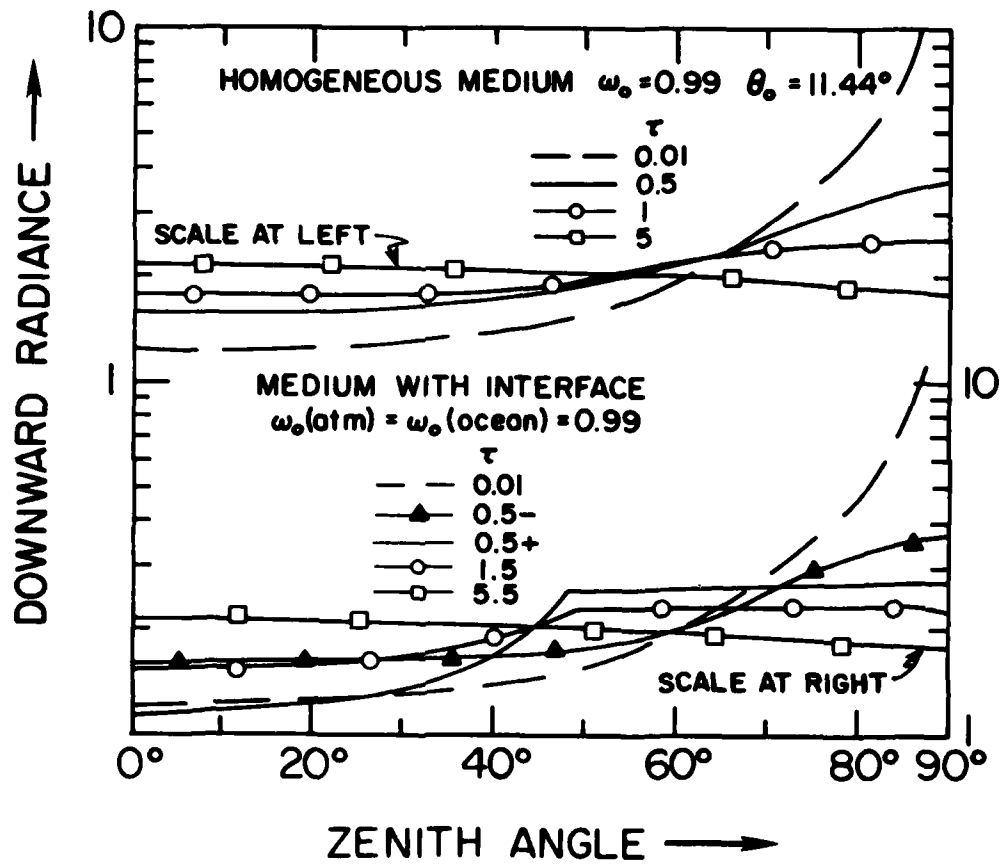


Fig. 9

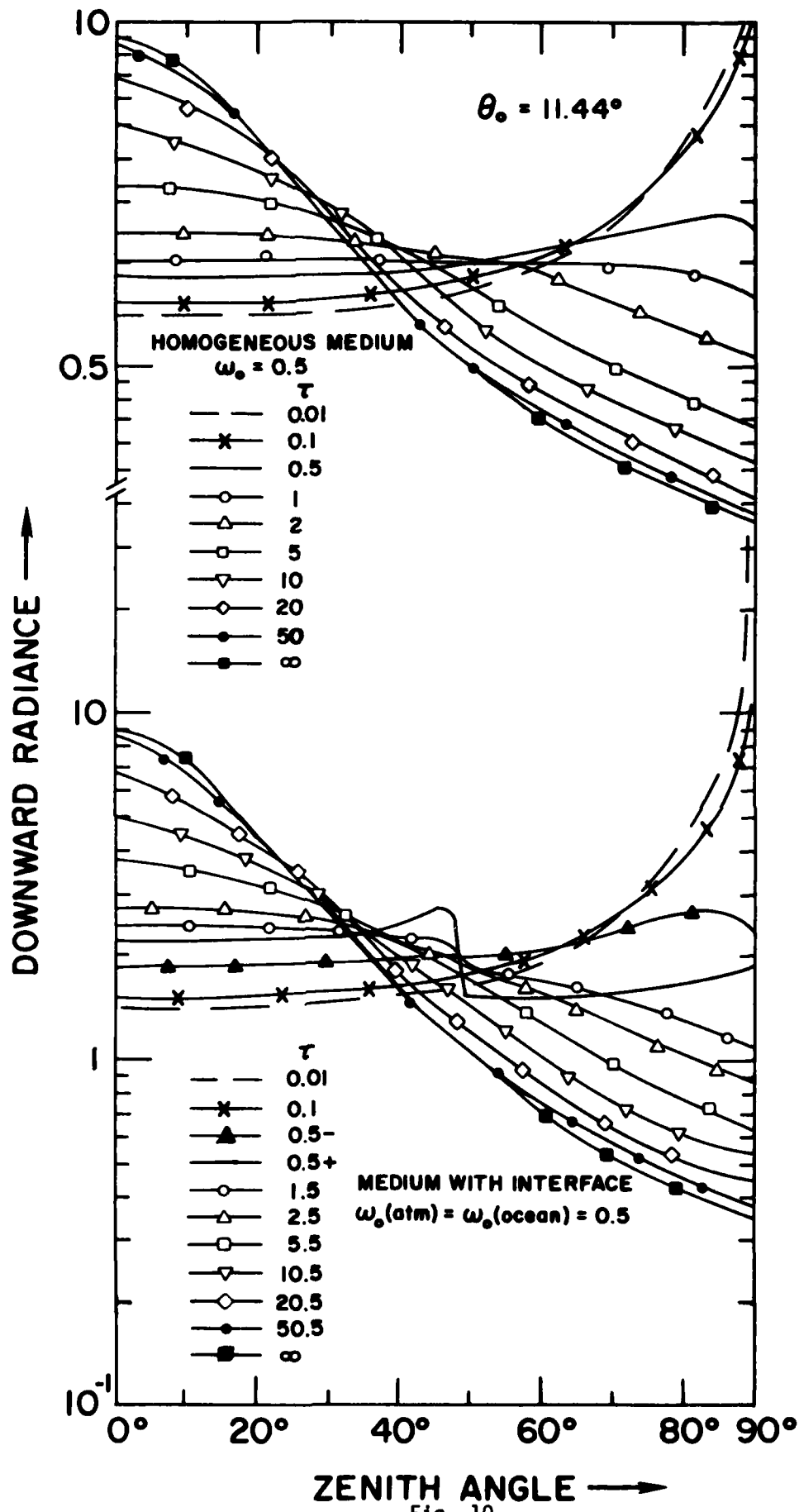


Fig. 10

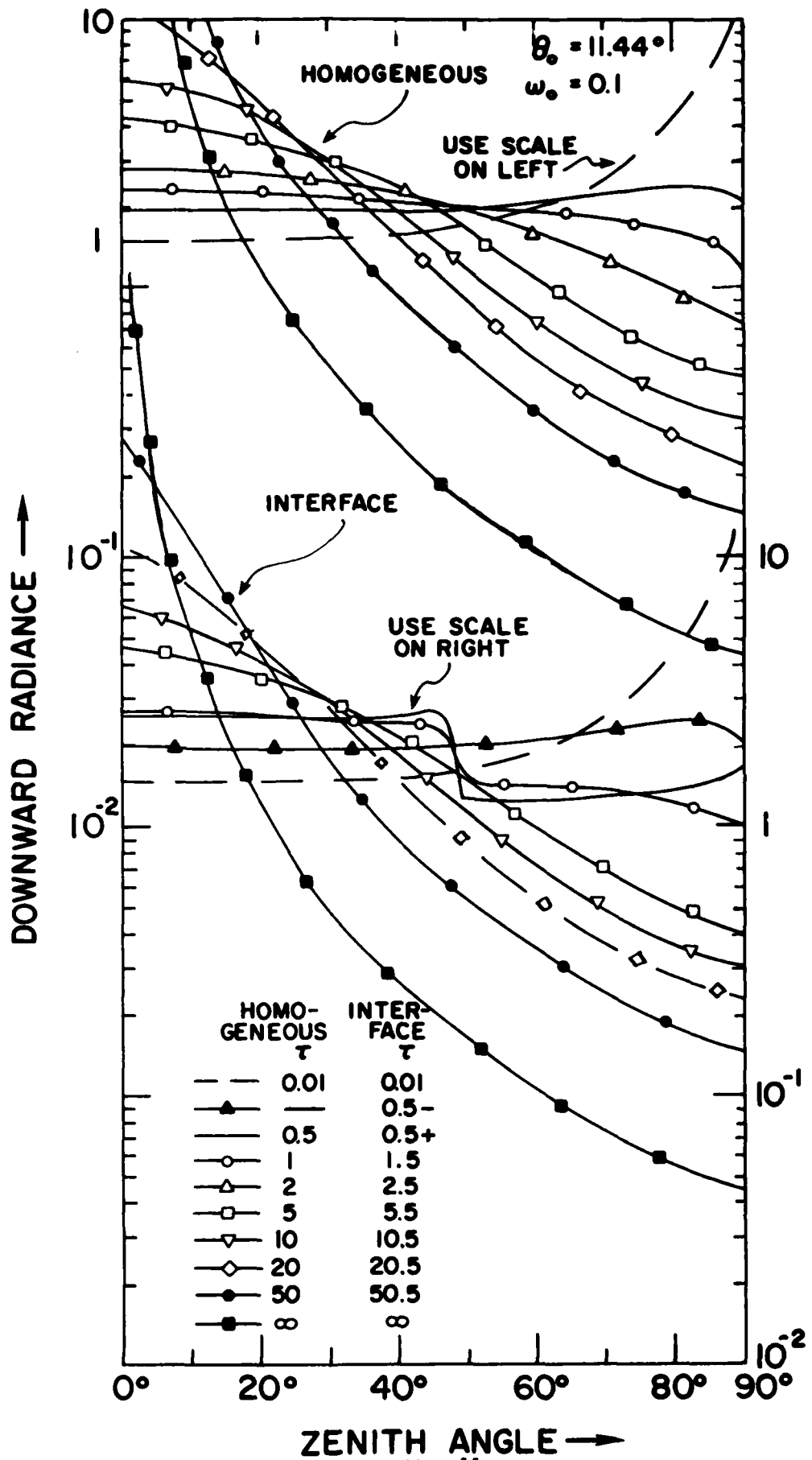


Fig. 11

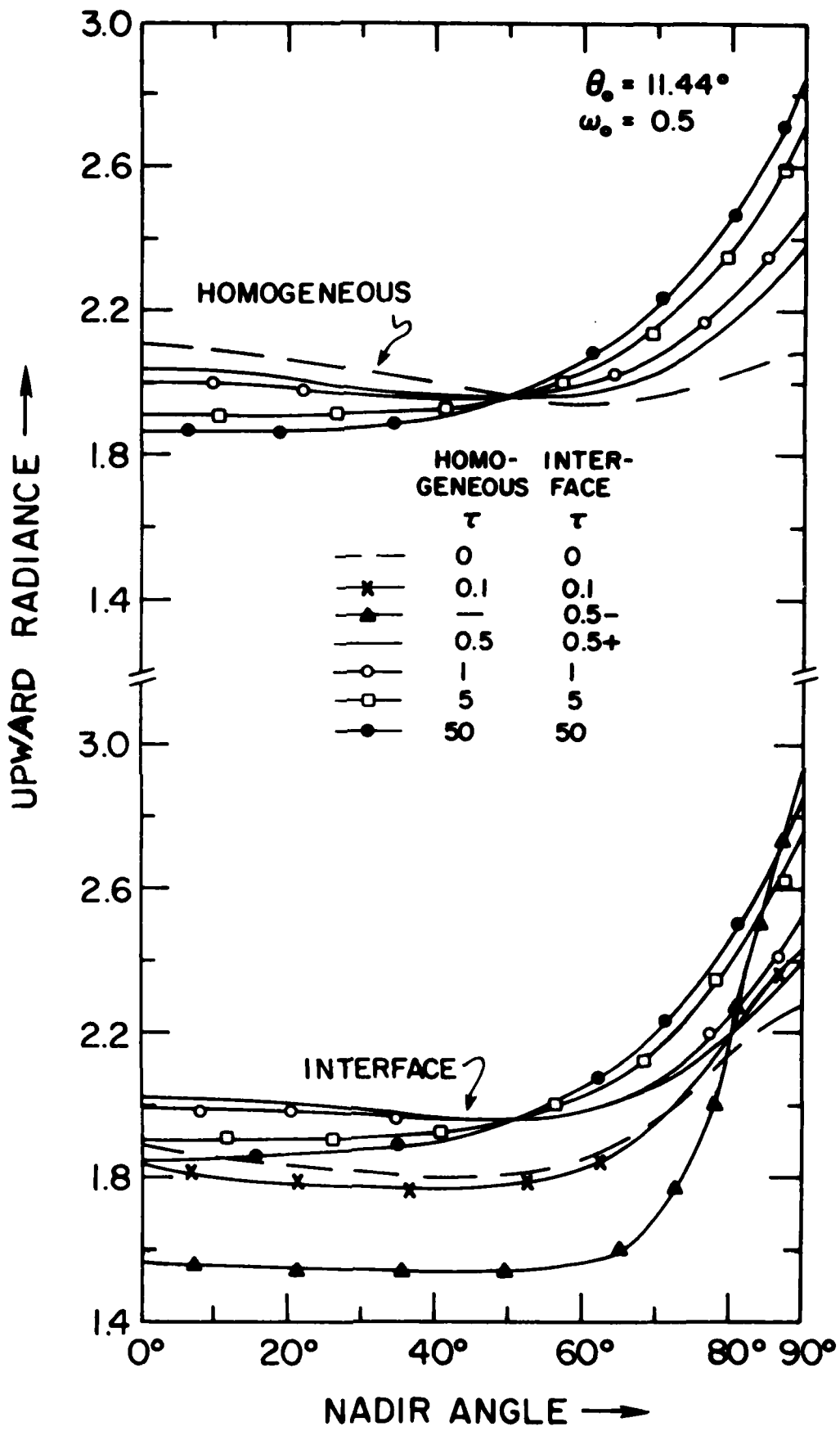


Fig. 12

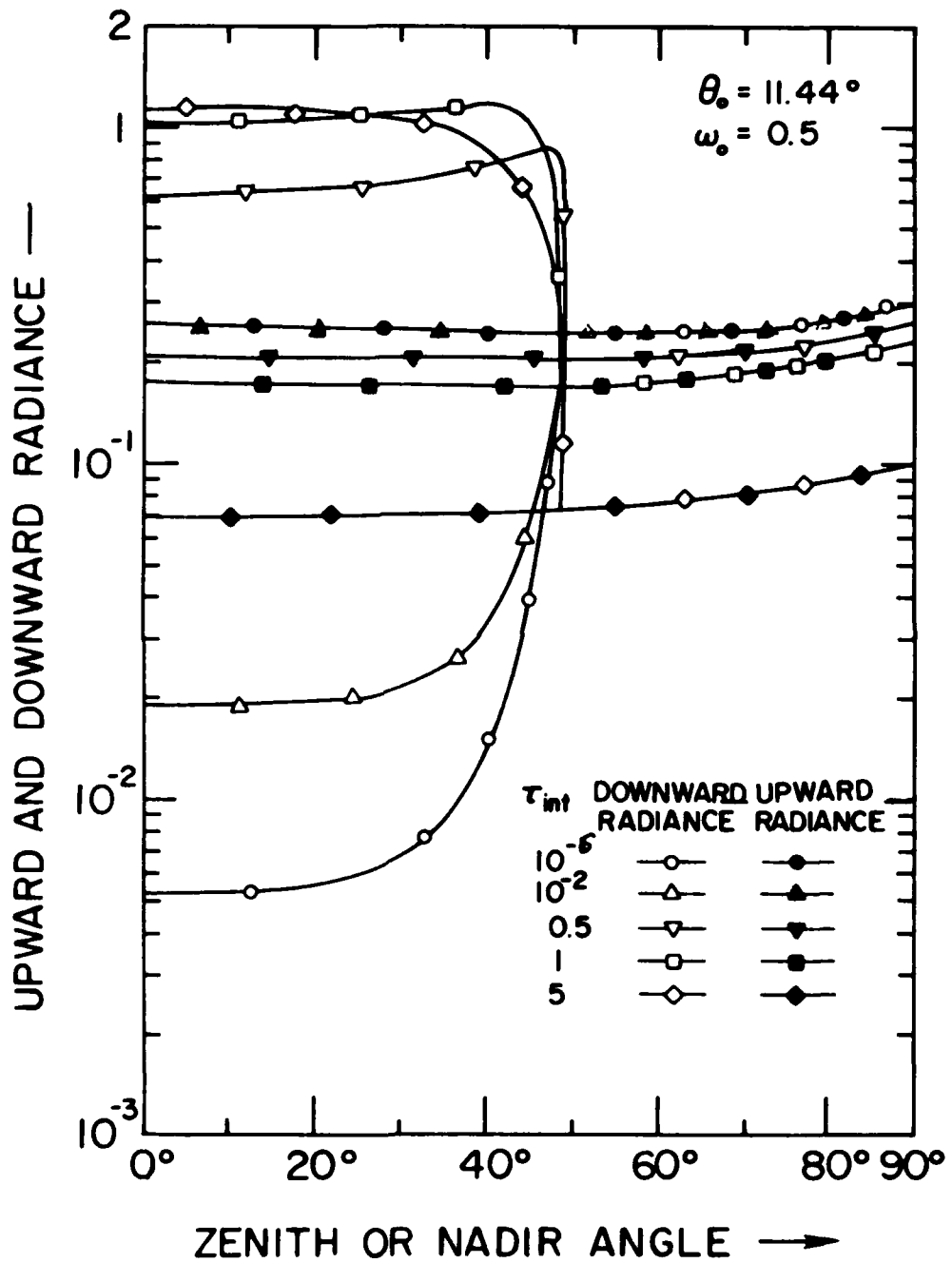


Fig. 13

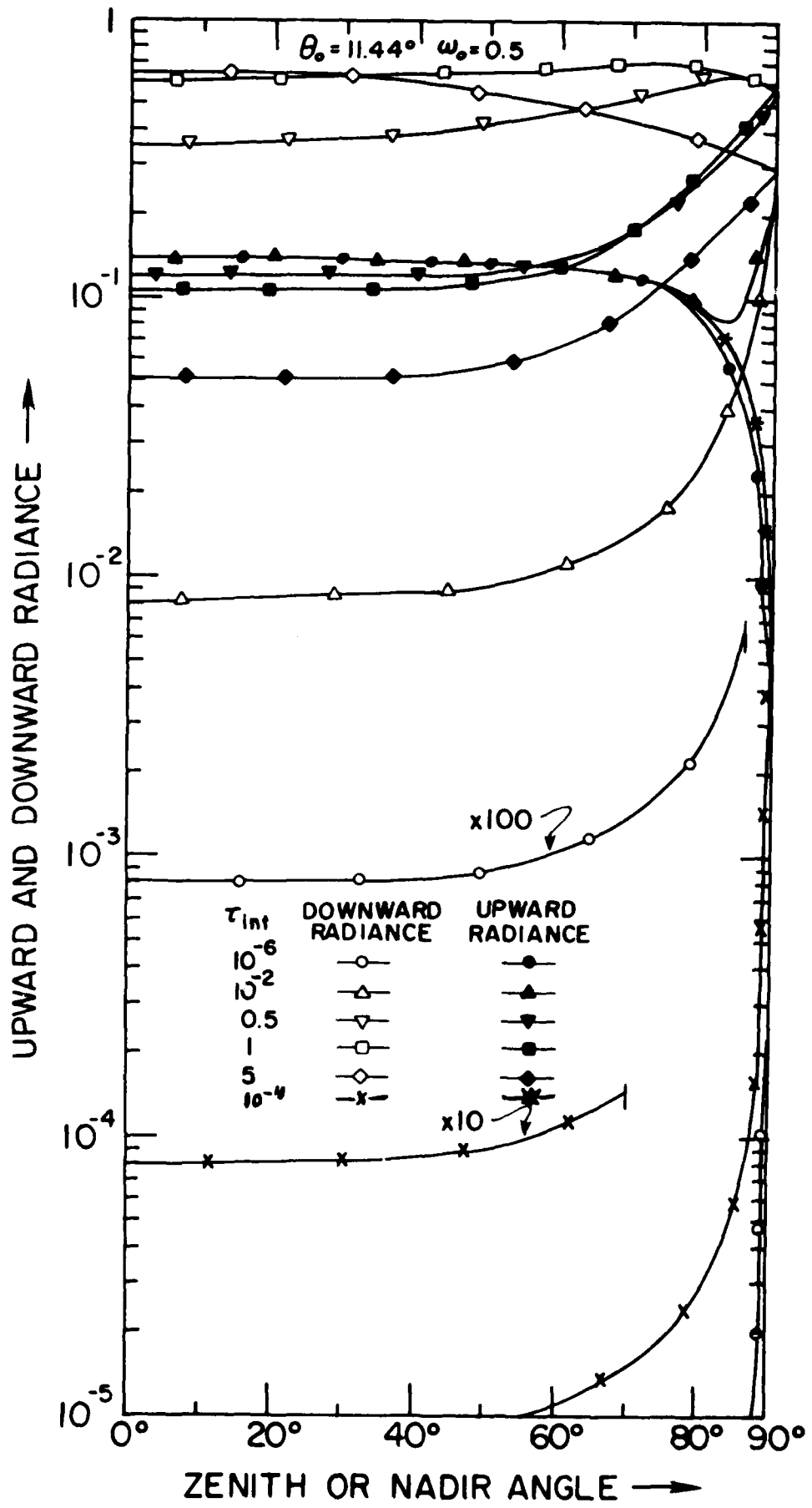


Fig. 14

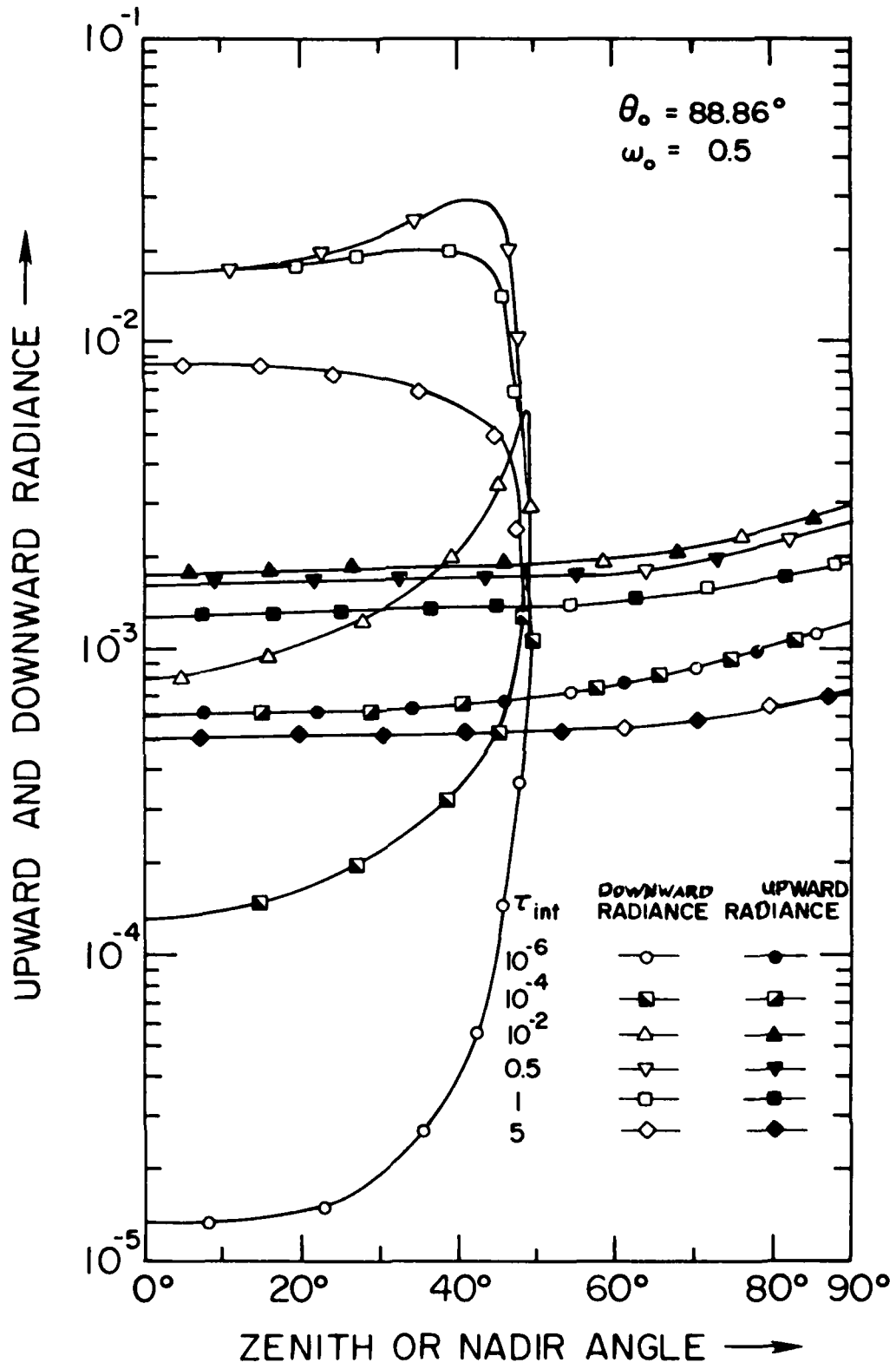


Fig. 15

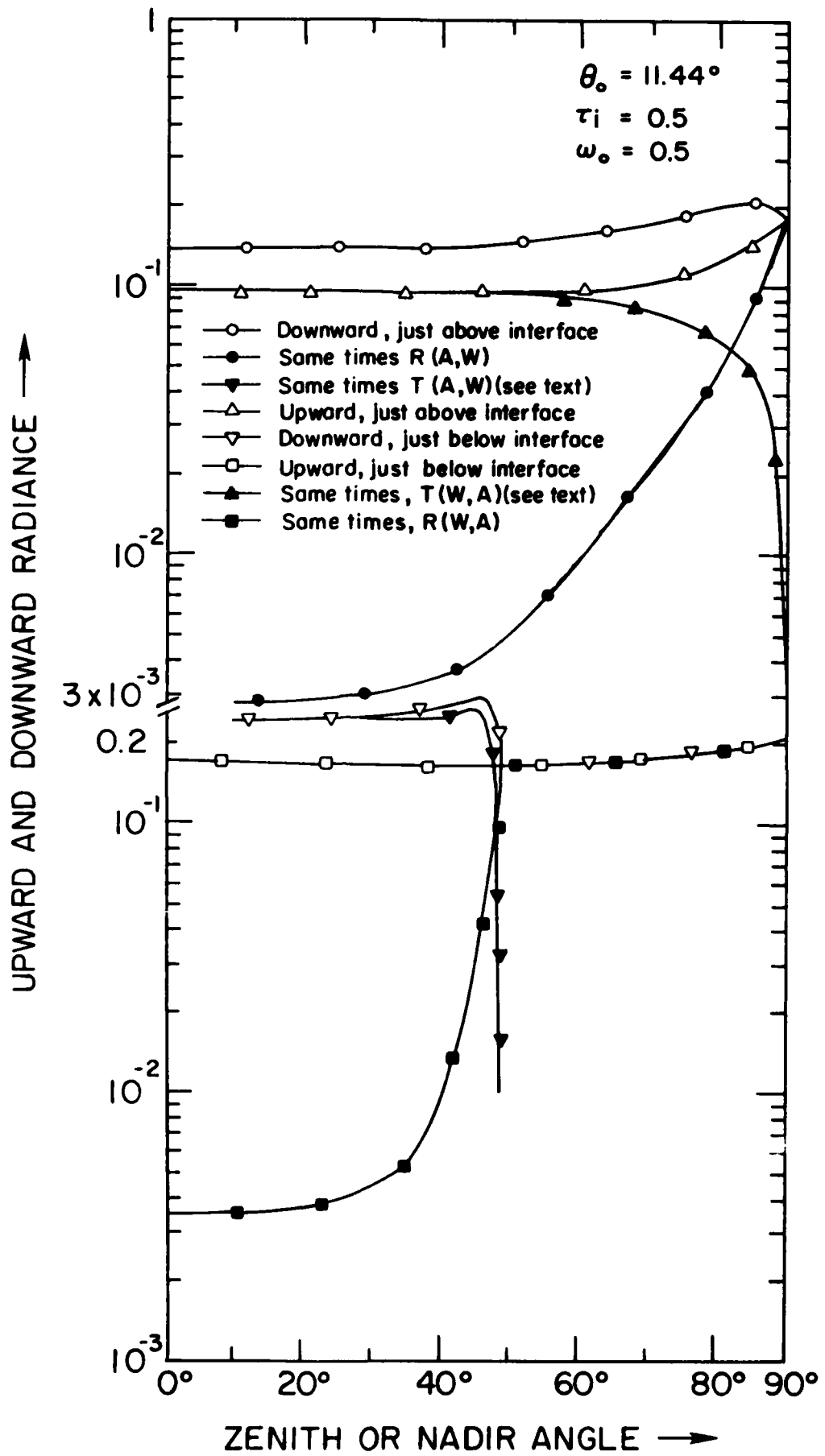


Fig. 16

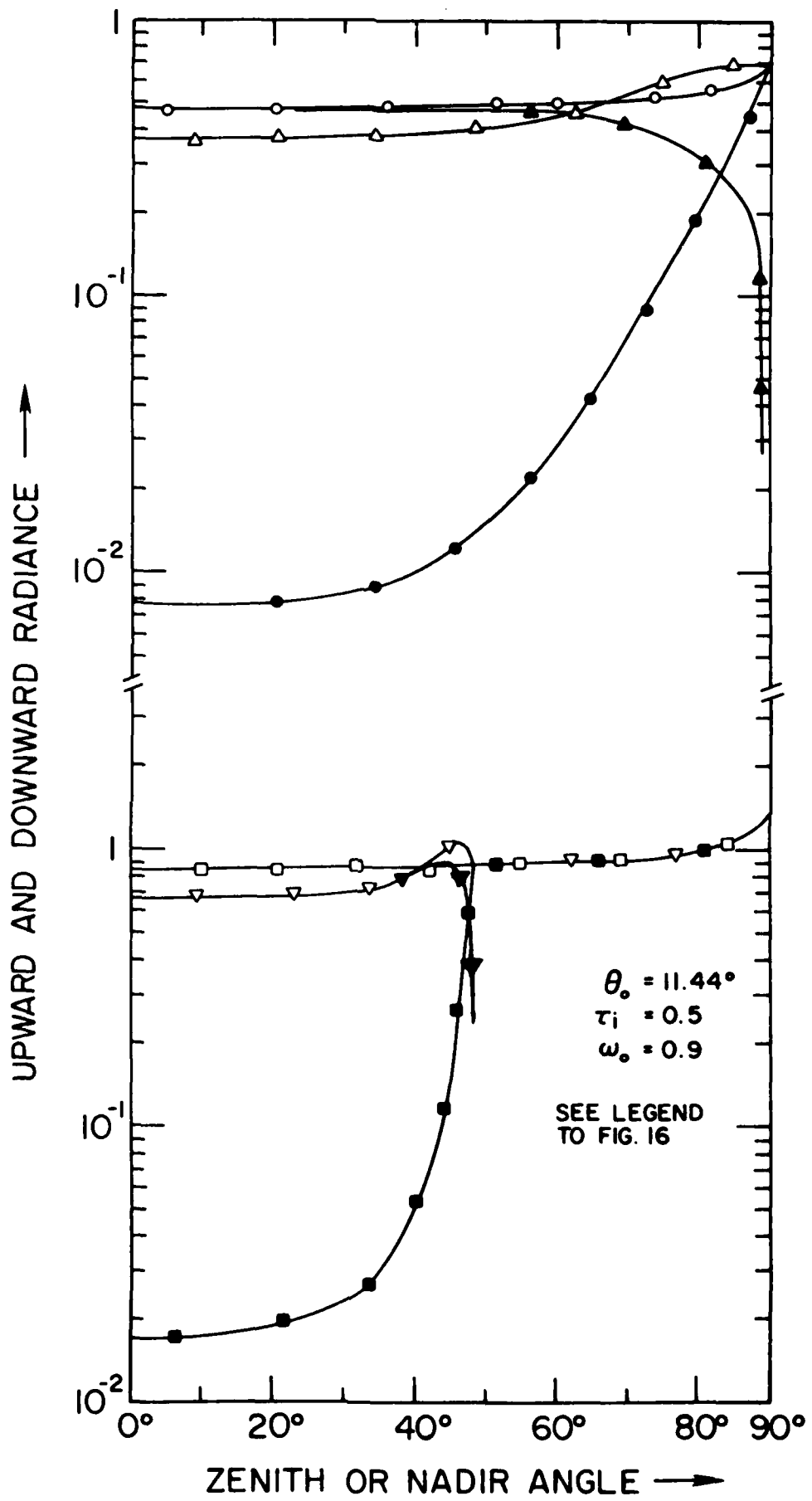


Fig. 17

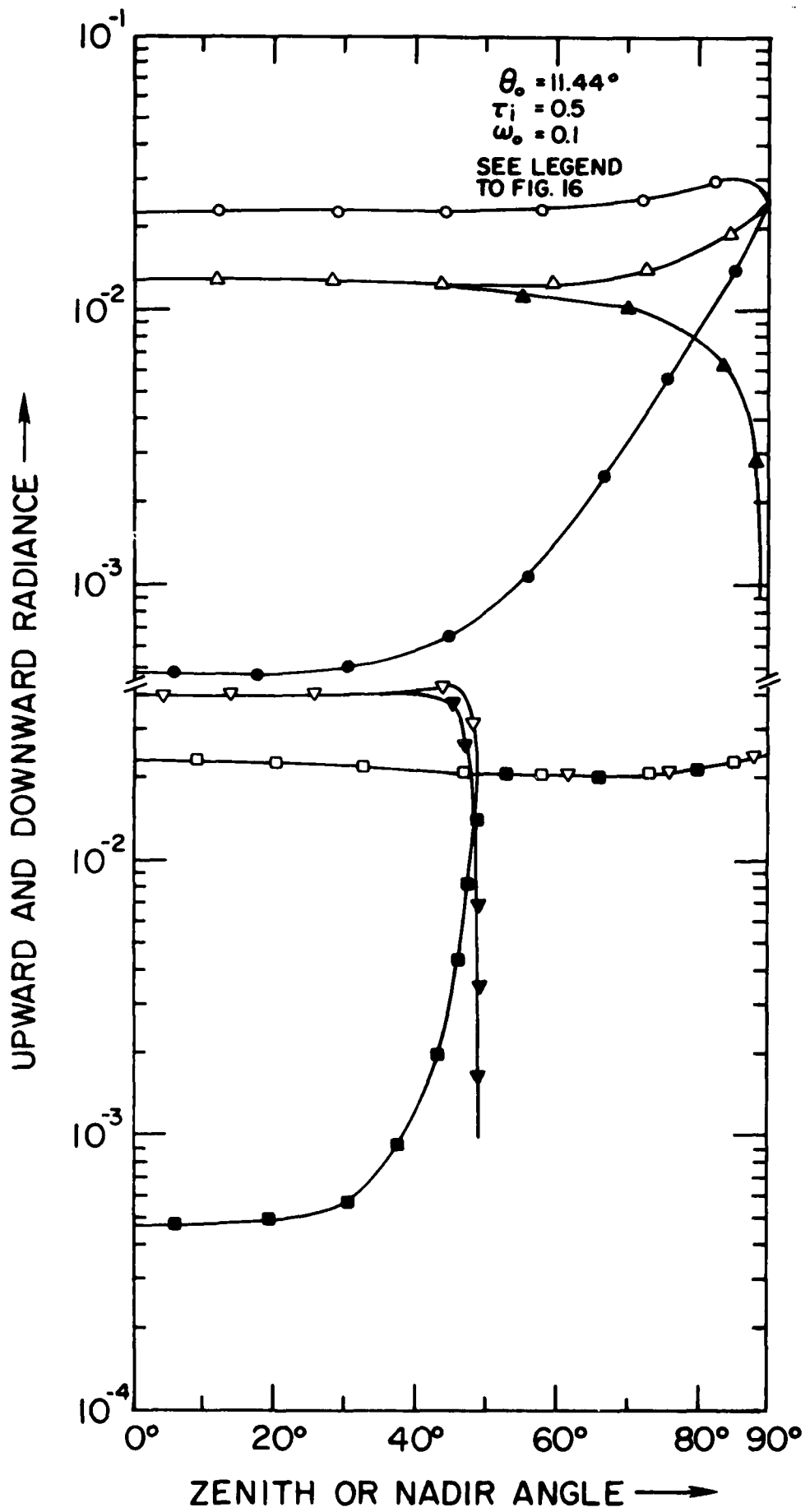


Fig. 18

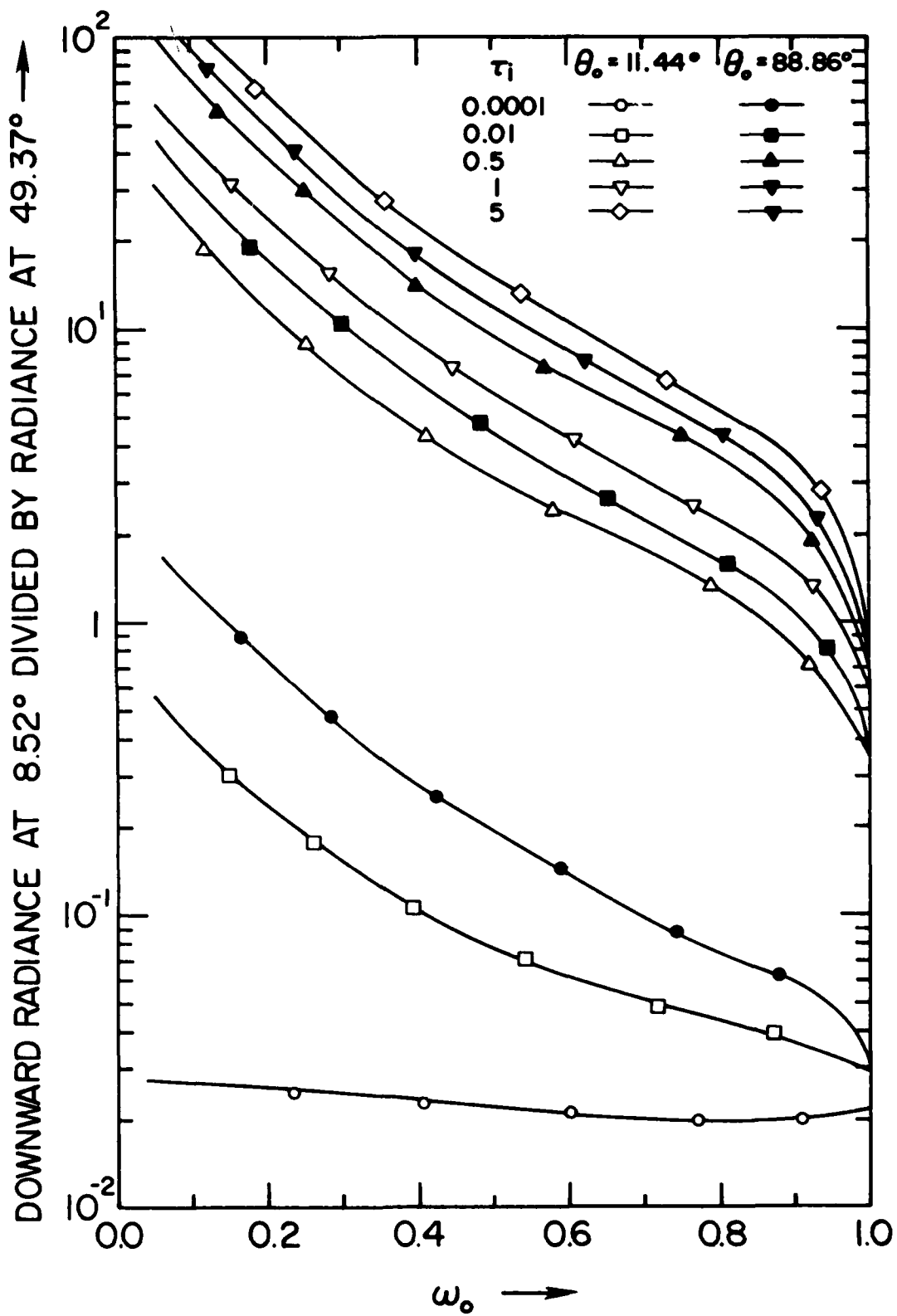


Fig. 19

MAXIMUM DOWNWARD RADIANCE
 DIVIDED BY RADIANCE AT 49.37° →

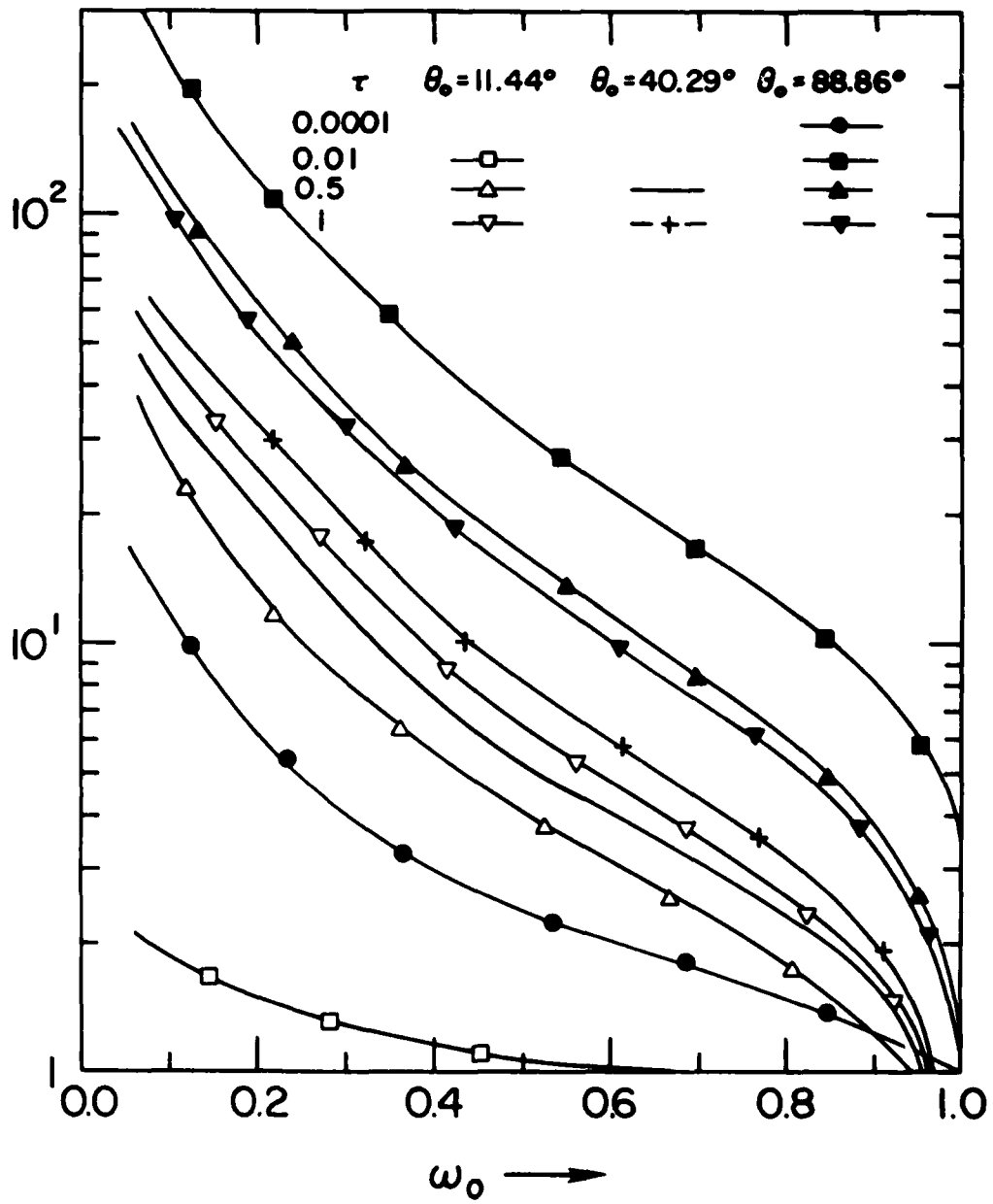
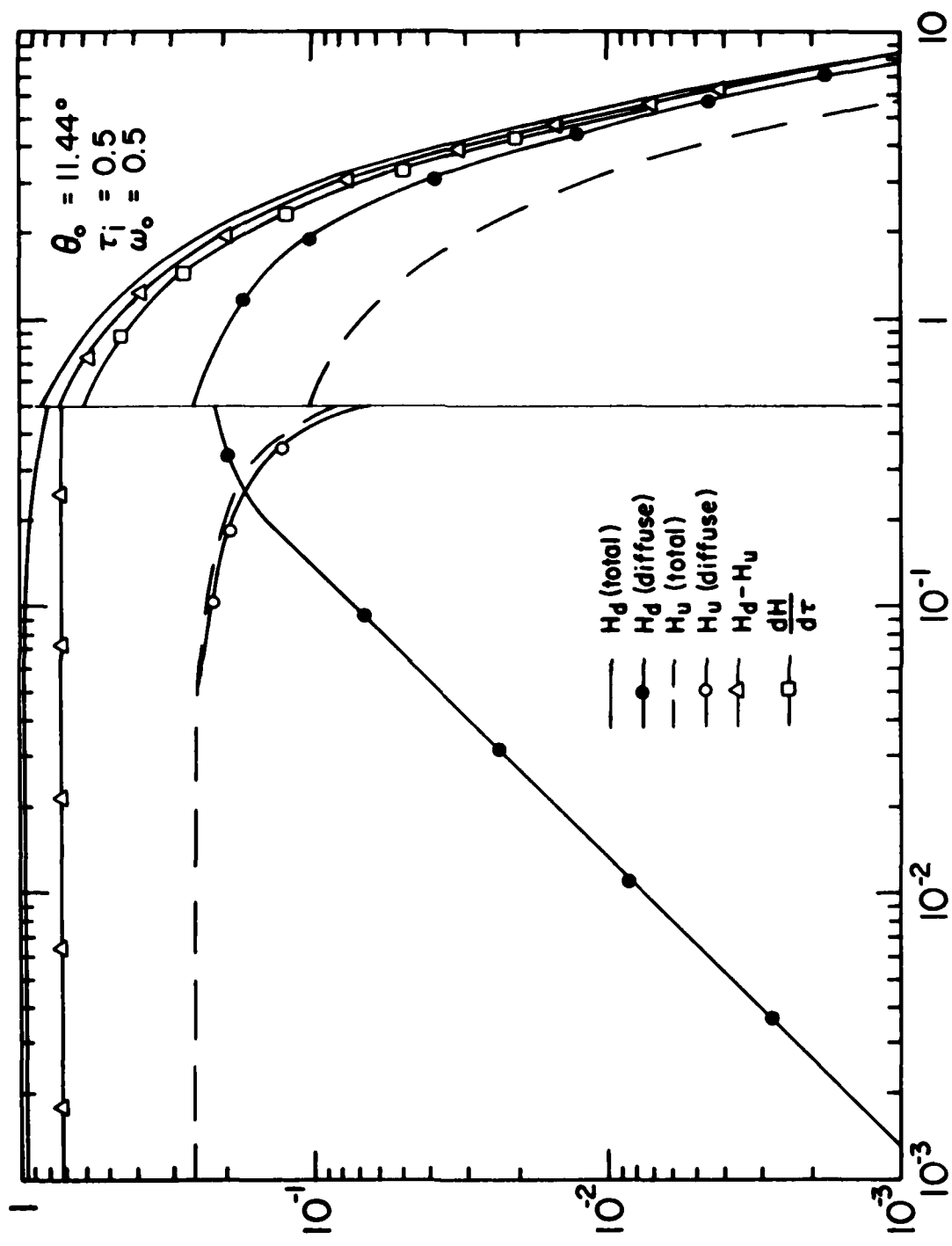


Fig. 20



$\tau \rightarrow$
 Fig. 21

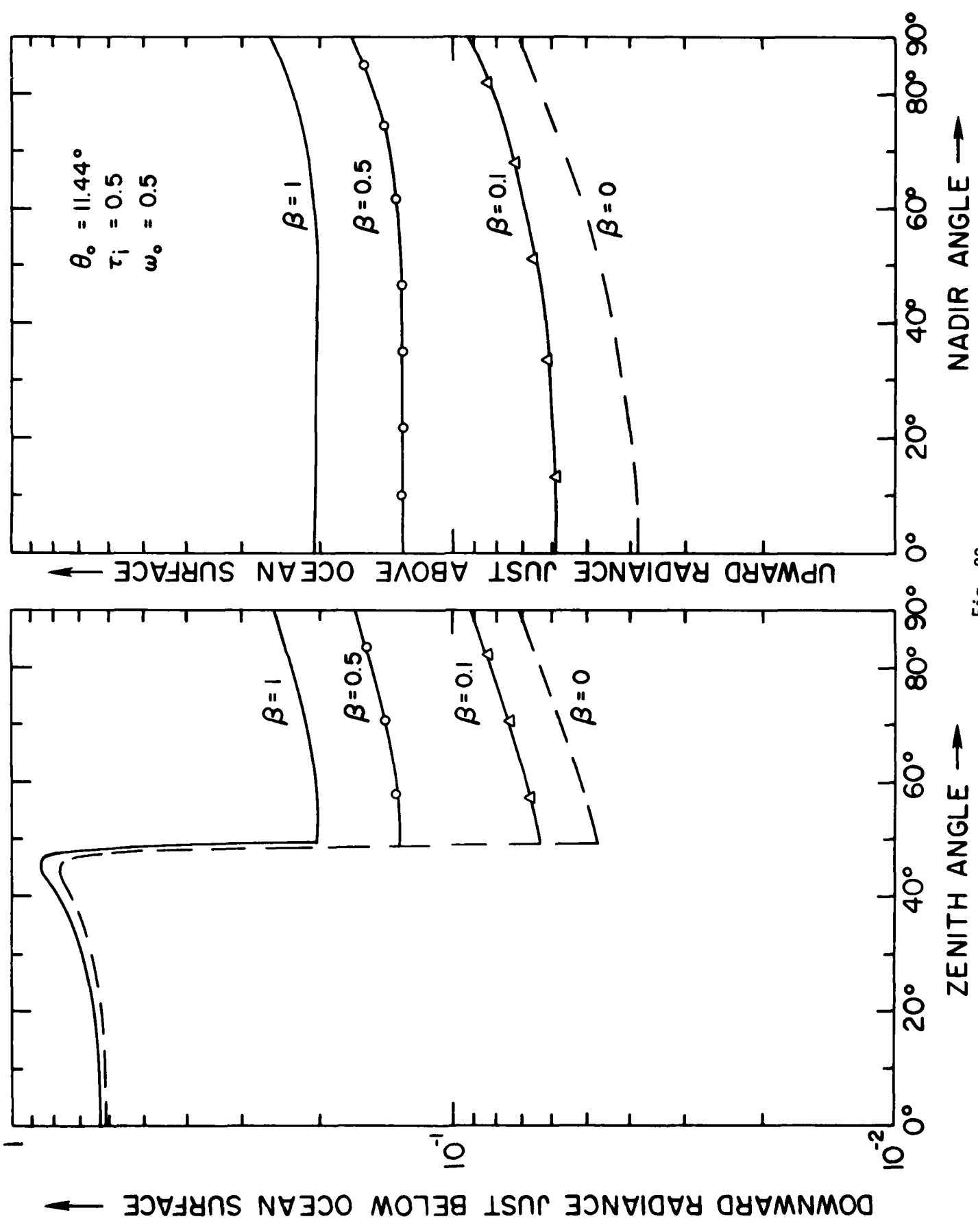


Fig. 22

DATE
FILMED
- 8